# Design and development of bladeless vibration-based piezoelectric energy-harvesting wind turbine

Younis, A., Dong, Z., ElBadawy, M., AlAnazi, A., Salem, H., & AlAwadhi, A.

2022

applied sciences

MDPI

*Article*

# Design and Development of Bladeless Vibration-Based Piezoelectric Energy–Harvesting Wind Turbine

**Adel Younis [1,*], Zuomin Dong [2], Mohamed ElBadawy [1], Abeer AlAnazi [1], Hayder Salem [1] and Abdullah AlAwadhi [1]**

[1] Department of Mechanical Engineering, Australian University, P.O. Box 1411, Safat 13015, Kuwait; m.elbadawy@ack.edu.kw (M.E.); a.alanazi@ack.edu.kw (A.A.); h.salem@ack.edu.kw (H.S.); a.alawadhi@ack.edu.kw (A.A.)

[2] Department of Mechanical Engineering, University of Victoria, P.O. Box 1700 STN CSC, Victoria, BC V8W 2Y2, Canada; zdong@uvic.ca

* Correspondence: a.younis@ack.edu.kw

**Abstract:** To meet the growing energy demand and increasing environmental concerns, clean and renewable fluid energy, such as wind and ocean energy, has received considerable attention. This study proposes a bladeless wind energy–harvesting device based vortex-induced vibrations (VIV). The proposed design is mainly composed of a base, a hollow mast, and an elastic rod. The proposed design takes advantage of vortices generated when the airflow interacts with the mast, and the flow splits and then separates and generates vortices that eventually make the elastic rod oscillate, and out of these oscillations, energy can be harvested. Different airflow disruption geometries are studied and tested numerically and experimentally to identify the most effective shape and orientation for converting wind energy to electric energy. Computational fluid dynamics (CFD) modeling and simulations were performed on the elastic mast, a VIV device's core wind energy–collecting component, to guide the device's design. These simulations examined the mast-produced lift coefficient, velocity, pressure, and vorticity contours of different mast geometries. The mast's vibration energy under different wind intensities was also experimentally tested using a scaled model in the wind tunnel. The level of converted electric power was measured and monitored using piezoelectric sensors mounted at different locations on the mast. The experimental study identified the ideal orientation angle of the mast and the best location for the piezoelectric sensors for harnessing more energy. The experiments confirmed the CFD simulation results that a complex cylinder design produces more power. The combined numerical and experimental studies led to an environmentally friendly, new VIV design with much improved power generation capabilities.

**Keywords:** wind energy; energy harvesting device; vortex-induced vibrations; computational fluid dynamics



**Citation:** Younis, A.; Dong, Z.; ElBadawy, M.; AlAnazi, A.; Salem, H.; AlAwadhi, A. Design and Development of Bladeless Vibration-Based Piezoelectric Energy–Harvesting Wind Turbine. *Appl. Sci.* **2022**, *12*, 7769. https://doi.org/10.3390/app12157769

Academic Editor: Georgios Papadakis

Received: 16 June 2022
Accepted: 28 July 2022
Published: 2 August 2022



## 1. Introduction

In recent years, there has been a spike in interest in exploring various environmentally friendly and renewable energy–harvesting designs that can address global energy and environmental concerns. The use of wind energy and the delivery of power for electronic devices via aeroelastic vibration has been studied. Some researchers have focused on collecting aeroelastic energy from aerofoils, while others have concentrated on converting energy created by vortex-induced vibrations (VIV). VIV is an energy harvesting method that uses the vortex shedding phenomena, in which an oscillating lift force is applied to a body, and the interaction between the fluid and the solid structure, which in practice is an elastic structure, allows engineers to generate electricity [1]. The VIV of a structure is often related to various engineering problems. For example, VIV can cause vibrations in heat exchanger tubes and change the dynamics of riser tubes that convey oil from the seabed

to the surface. VIV also has ramifications for marine and land vehicle design and causes large-amplitude vibrations in anchored structures in the ocean. On the positive side, a long cylinder mounted on a flexible structure can be used to gather energy created by VIV. The cylinder is susceptible to vortices that regularly shed, causing transverse vibrations. The vibrations can then be transformed into electric power using piezoelectric generators mounted on the cylinder. Most VIV harvesters have a narrow output band around wind speed, where the structure's inherent frequency equals the vortex shedding frequency.

The presence of real-world scenarios such as the vibrations of offshore structures and riser pipes, building vibrations, and fluid movement in a heat exchanger, among others, has generated interest in studying VIV. VIV was initially thought to have harmful effects. The viscous effects of a fluid flowing over a cylindrical body, for example, separate it from the surface. When the liquid separates from the surface, new forces emerge on the surface, which are large enough to cause the structures to vibrate, triggering them to break. A thorough understanding of the nature of VIV from a design standpoint is required to use these vibrations to create energy and avoid technical failures. While aeroelastic resonance is considered a nuisance, it provides the technological underpinning of wind energy conversion.

Over the last two decades, several researchers have investigated the problem of harvesting energy from flow-induced vibrations [2,3]. In an experimental context, Li et al. [4] examined a bio-inspired leaf architecture that transfers wind energy into usable electric power. In addition, energy harvesting devices were proposed by Abdelkefi et al. [5] and Jung and Lee [6] employing piezoelectric and electromagnetic transduction technologies with vibrations produced by wake galloping.

Lock-in or synchronization of VIV happens when one of the inherent frequencies of the dynamic design equals the frequency of vortex shedding, resulting in vortex-induced vibrations (VIVs). Through experiments, Akaydin et al. [7] employed flexible piezoelectric material under VIV for energy gathering. Mehmood et al. [8] investigated energy harvesting from circular cylinder VIV. Abdelkefi et al. [5] investigated the effects of Reynolds number and electrical load resistance on the lock-in zone as well as the performance of the energy harvester. Finally, Akaydin et al. [9] conducted another experiment in which the energy harvester's output performance was investigated by altering the flow speed and testing the self-excited energy harvester subjected to uniform cross flows. Based on the experimental work of Akaydin et al. [9], Dai et al. [10] developed a theoretical distributed-parameter model and used the Euler–Lagrange method to achieve reasonable agreement with the experimental results. Another comparison study was undertaken by Dai et al. [10] on four alternative orientations of the circular cylinder while subjected to vortex-induced vibrations, including tests for different wind speed areas for each harvester design. They also recommended the best orientations for various wind speeds. Variations in wind speed cause the obtained energy levels to drop substantially due to the restricted range of the synchronization region, which is a severe setback for energy collection. This setback restricts VIV energy harvesting's ability to achieve efficient performance and the intended design. As a result, scientists are working on novel approaches to creating broadband energy harvesting systems susceptible to flow-driven vibrations or base harmonic excitations. The foundation of these solutions is the use of external axial loading or magnetic forces to introduce nonlinear restoration forces. These new nonlinear forces increase power generation by hardening or softening behavior, resulting in a wide range of resonant frequencies. Structures can be monostable or bistable depending on the magnitude of the force due to the buckling instability generated by these nonlinear features. The biostable structure is reported to produce broadband resonant regions for base-excited energy harvesters. Furthermore, Masana and Daqaq [11] demonstrated that multiple acceleration levels are required to activate the biostable configuration to produce too-vast broadband resonant regions. R. Naseer et al. [12] used vortex-induced vibrations in a study in which two sets of attracting magnets were positioned so that the harvester could be buckled to extend the synchronization zone and enhance the power-collected performance

level. Sun and Wang [13] introduced magnetic force to design a bi-directional U-shaped piezoelectric energy harvester for vortex-induced vibrations. They claimed that by adding magnets to their design, significant improvement of the lock-in region and the peak voltage were noticed. Dai et al. [14] constructed a set of representative coupled equations that account for the transverse displacement of the bluff body and the induced electromagnetic current. Nonlinear analysis was also performed in their study to investigate the effects of the electrical load resistance and wind speed on the harvester's outputs. Marqui and Erturk [15] analyzed two airfoil-based aeroelastic energy harvesters using piezoelectric transduction and electromagnetic induction. Adding piezoelectric and electromagnetic couplings, they investigated an airfoil with two degrees of freedom. Minazara et al. [16] developed a piezoelectric generator that harvests mechanical vibration energy on a bicycle. Jayarathne et al. [17] developed a vibration energy–harvesting device using the cantilever-type configuration to harvest vibration energy from vehicles. Lead zirconate titanate (PZT) was selected as the piezoelectric material.

Ishihara and Li [18] investigated the mechanism of suppression for VIV of circular cylinder by helical wires using the LES turbulence model. Numerical models for free-vibrating circular cylinders with and without helical wires were presented and experimentally validated. The steady and unsteady aerodynamic forces of circular cylinders with and without helical wires were examined to clarify the mechanism of VIV suppression in their study. Li and Ishihara [19] investigated the wake galloping of tandem circular cylinders using the LES turbulence model. They proposed a numerical model for a transversely free-vibrating circular cylinder in the wake of another fixed cylinder and validated its accuracy. They also examined the flow patterns and the characteristics of wake galloping and dynamic fluid forces on the downstream cylinder to clarify the effect of mass and spacing ratios.

This paper utilizes wind energy power generation using VIV-based fluid-structure wind interaction technology to avoid the trouble-prone mechanical shafts and gears in conventional wind turbines. The rigidity of the resonant structure can be modified by applying magnetic forces to it, increasing the operational life and applicable wind speed range. The energy from the rhythmic movement can be converted into electricity using electromagnetic induction.

This paper aims to develop a VIV wind energy–harvesting device that converts mechanical energy (vibrations) to electric energy. The proposed device generates energy while utilizing aeroelastic resonance phenomena. The device is bladeless and has an elastic rod that oscillates when the frequencies of both the material of the elastic rod and the airflow become equal. The device uses piezoelectric sensors located at three different locations to harness energy. Different geometrical designs were used to gauge the performance of each and determine the optimal shape/geometrical design that may increase the harvested energy. In the following section, the design methodology of the suggested design is introduced.

## 2. Design Methodology

The design methodology of the proposed design can be explained in the following statements. When a steady fluid flow is applied to an elastic bluff body at high enough Reynolds numbers ($R_e$ > 100), the flow breaks from the body surface, resulting in an unsteady broad wake. Two unstable shear layers on each side of the body roll up to form vortices, which characterize the flow pattern. These vortices that were produced lead to oscillation (mechanical energy), which is then converted to electric energy through the components of the proposed energy harvesting device. The undisturbed flow speed $U$ and the size of the cross-sectional body $D$ are connected by the well-known Strouhal relationship, $S_T = \frac{f_T D}{U}$, and with a frequency of $f_T$, these vortices are shed to the wake periodically. The frequency of vortex shedding increases as the flow velocity increases from zero, and there is a flow velocity at which vortex shedding has a frequency close to the body's natural frequency of oscillations $f_N$, and significant oscillations can be induced

in the body for low mass and mechanical properties. When a body oscillates, it creates a complex interaction with the flow field surrounding it, which has two unique features: (i) a range of flow velocities exists where the vortex shedding frequency is synced with the oscillation frequency (lock-in regime), resulting in large oscillations; and (ii), with jumps in oscillation amplitude and the fluid forces acting on the body, the cylinder response may exhibit hysteresis. The proposed design incorporated these two qualities. However, at low wind speed, achieving a frequency where $f_T$ equals $f_N$ remains a challenge that the proposed design in this study should be able to address.

The wind flow is incompressible with constant density, and the effect of viscosity is negligible far from the walls of the VIV design in this study.

The conservation of mass and momentum equations are the most fundamental equations in every fluid flow domain. However, according to the turbulent nature of wind flow in this study, the momentum equation should be written so that the effect of turbulent stresses is considered. Therefore, the conservation of mass seen in Equation (1) and the conservation of momentum (the Cauchy equation) Equation (2) were utilized in this work, as follows:

$$\frac{\partial \rho}{\partial t} + \nabla \cdot (\rho \mathbf{u}) = 0 \tag{1}$$

$$\frac{\partial (\rho \mathbf{u})}{\partial t} + \nabla \cdot (\rho \mathbf{u}\mathbf{u}) = -\nabla p + \nabla \cdot \tau \tag{2}$$

where $\rho$ is the density, $t$ is time, $\mathbf{u}$ is the velocity field, $p$ is the pressure, and $\tau$ is the turbulent stress tensor and would be calculated based on the selected model in the CFD software.

Solving these equations, the Lift coefficient is attainable, which is necessary for power generation calculations as in Equation (3):

$$C_L = \frac{F_L}{\frac{1}{2}\rho U^2 A} \tag{3}$$

where $F_L$ is lift force; $A$ is reference area, and $U$ is freestream velocity.

Also, the Strouhal number ($St$), which is mandatory for finding vortex shedding frequency, can be calculated using Equation (4).

$$St = \frac{fL}{U} \tag{4}$$

where $St$ is the Strouhal number, $f$ is the vortex shedding frequency, and $L$ is the characteristic length.

The harvested power of the VIV device can be determined using Equation (5), considering the defined parameters and their values reported in Table 1:

$$\overline{P} = \frac{\omega^2 b^2 h^2 e_{31}^2 \overline{A}^2 R}{4(1 + bL\varepsilon_{33}\omega R/\Delta)^2} \tag{5}$$

**Table 1.** Design parameters.

| Parameter | Piezoelectric Sensor | Host Beam |
|---|---|---|
| $L$: Length (m) | 0.064 | 0.35 |
| $b$: Width (m) | 0.02 | 0.032 |
| $t$: Thickness (m) | 0.0019 | 0.0008 |
| Modulus of elasticity: E (Pascal) | | $2.00 \times 10^{14}$ |
| I ($m^4$) | | $1.37 \times 10^{-12}$ |
| e31 (coulomb/$m^2$) | −10.4 | |
| e33 Relative permittivity (F/m) | 0.0000008 | |
| Vibration amplitude: $A$ (m) | 0.004 | |
| Resistance: $R$ (Ohm) | 4000 | |

**Table 1.** *Cont.*

| Parameter | Piezoelectric Sensor | Host Beam |
|---|---|---|
| Buoyancy force (N) | 1 | |
| Mass of floating objects (kg) | $2.50 \times 10^{-1}$ | |
| Beam natural frequency: $\omega$ (HZ) | $4.40 \times 10$ | |
| Supply voltage: | 3.3 V to 5 V | |
| Working current: | <1 mA | |
| Working temperature range | −10 °C–+70 °C | |

The following section provides the suggested VIV design model, including component descriptions and specifications, design calculations for the forces the device will encounter when interacting with wind, and harvested power calculations.

*The Proposed VIV Design*

This section displays the suggested design geometry and structure. While still linked to the bottom rod, the outer cylinder should be mostly stiff and able to vibrate. The top of the cylinder is unbound, and the amplitude of its oscillations is the largest. The structure comprises polymers reinforced with carbon and/or glass fiber, commonly utilized in wind turbine blades. The mast is supported at the top of the rod, while the bottom is firmly attached to the ground. It is made of a carbon fiber–reinforced polymer with excellent fatigue resistance and minimal energy leakage when oscillating. Naturally, the design of such a wind turbine is much different from that of a traditional turbine. The energy collecting design shown in Figure 1 is proposed in place of the typical tower, nacelle, and blades.

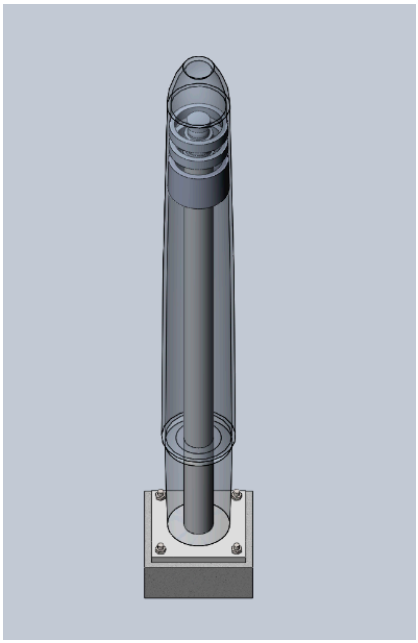

**Figure 1.** The preliminary proposed VIV design (manufacturing tolerances ± 0.1 mm, ISO.).

Table 2 displays a list of the components utilized in the proposed VIV device design, together with their descriptions and materials:

**Table 2.** The proposed design components and specifications.

| ITEM No. | Part Name | Description | Quantity | Material |
|---|---|---|---|---|
| 1 | Base | H 182 mm; L 455.24 mm; W 455.24 mm | 1 | Steel grade A36 |
| 2 | Elastic Rod | H 1202.6 mm; D 32.28 mm | 1 | Carbon fiber–reinforced polymer |
| 3 | Hollow Mast | H 2194.5 mm; OD 300 mm; ID 280 mm | 1 | Carbon fiber–reinforced polymer |
| 4 | Alternator | H 48.54 mm; OD 247.32 mm; ID 203.7 mm | 2 | Electromagnetic coil |
| 5 | Stator | H 203.68 mm; D 143.79 mm | 1 | Carbon fiber–reinforced polymer |
| 6 | Stator Support | H 2203.18 mm; D 123.54 mm | 1 | Carbon fiber–reinforced polymer |
| 7 | Hollow Mast Base | H 512.95 mm; OD 262.32 mm; ID 123.54 mm | 1 | Carbon fiber–reinforced polymer |
| 8 | Anchor Support | H14.57 mm; OD 44.57 mm; ID 23.67 mm | 4 | Steel grade A36 |
| 9 | Inner Ring | H 175.21 mm; OD 254.29 mm; ID 207.48 mm | 1 | Magnet |

Figure 2 presents the proposed design and the locations of the piezoelectric sensors that convey readings of harnessed energy at three different locations as soon as the elastic rod starts to oscillate due to airflow–structure interactions.

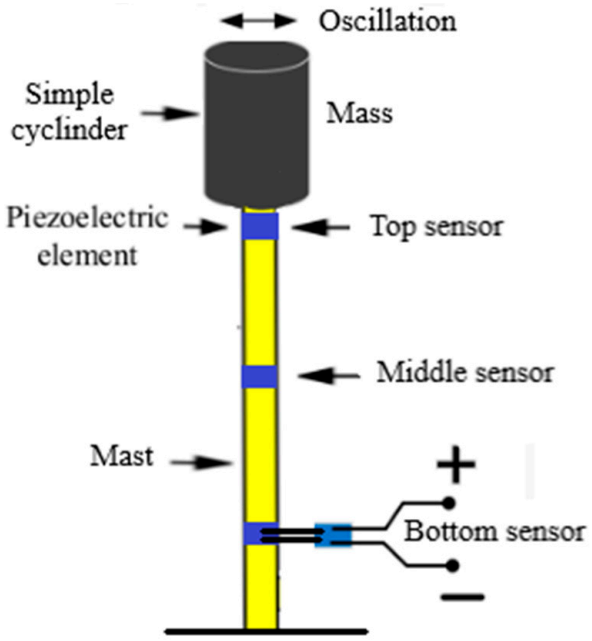


**Figure 2.** The proposed design with locations of piezoelectric sensors.

Table 3 displays the sensor sensitivity information used in this work. Three sensors were mounted on each design. They were tested at room temperature (25 °C)

**Table 3.** Sensor sensitivity information.

| Sensor Features | Sensitivity Information Range |
|---|---|
| Supply voltage (V) | 3.3~5 |
| Working current (mA) | <1 mA |
| Working temperature range (°C) | −10~+70 |

## 3. Computational Fluid Dynamics (CFD) Simulation Results

The work in this part is targeted at applying a computational fluid dynamics (CFD) approach to simulate vortex-induced vibrations of the flexible rising rods (mast). The current CFD capabilities may produce results that are reasonably close to the experimental data and may be used to calibrate existing low-order analytical models and provide a generic framework for various flow characteristics and boundary conditions. CFD flow models of numerous hollow mast designs were examined based on a theoretical review of

these designs. CFD is utilized to visualize the flow patterns, while the experimental work is conducted to be able to measure the amount of harvested energy, in addition to verifying the CFD results. The following section describes the wind flow trajectories and pressure distribution on the hollow mast. Different hollow mast designs with various diameters and heights were explored, and CFD results are presented in this section.

Based on the experimental results, which showed that 15 m/s is the airflow speed where a good amount of energy can be generated, a lower wind speed of 10 m/s and a higher wind speed of 20 m/s were chosen to focus on in addition to 15 m/s. The step size of 5 m/s was chosen based on that fact that there is no significant change when the speed step size is smaller than that. In Appendix A, Tables A1–A4 display the experimental results with a step size of 1 m/s, which proves that there is no significant change when the step size is small.

The convergence criterion should be the first thing to check the convergence of the executed simulation. It helps in understanding the global and local imbalances in an iterative way in a CFD simulation. In this paper, residuals that represent the solution imbalances were considered as the convergence criterion to check for numerical accuracy. Residuals are expected to be as small as possible to indicate the accuracy of simulations. Residuals below $1 \times 10^{-3}$ were taken as a good starting point to move to the next check.

The results of the CFD simulations for two different geometries (simple cylinder and complex cylinder) at a wind speed of 10 m/s are presented. Figure 3 shows the vorticity contours for simple cylinders and complex cylinders, respectively. It can be noticed that the complex cylindrical shape produced more flow disturbance and intensive vortices. This essentially motivates the mast to vibrate and, hence, produce energy.

Figure 3 below shows CFD simulation results and a comparison of two different shape designs. In addition, the velocity, pressure, and vorticity contours for both the simple cylinder and modified cylinder designs at wind speed equal to 10 m/s were investigated and are presented in Figure 3. CFD simulations revealed that the modified cylinder design at low wind speed yields no difference from the simple cylinder design. This indicates that a modified cylinder design at low wind speed (10 m/s) may not produce as much oscillation as intended.

In Figure 4, the wind speed increased to 15 m/s, and CFD simulations were carried out to study the effect of changing the wind speed and the design shape. The simulation results shown in Figure 4 show that when the wind speed is increased, the effect becomes evident that more pressure and more intense vortices are generated. Hence, more oscillations and more power are generated. It becomes even better when the wind speed goes up to 20 m/s, as shown in Figure 5. More pressure contributes to increasing lift forces that are translated as oscillations and more intense vortices, indicating turbulence that causes more vibrations in the design and generates more energy. CDF simulation results showed that the investigated two factors, geometrical design shape and wind speed, play a significant role in creating the oscillations and vibrations that produce more energy. Therefore, it can be concluded that complex cylindrical design shapes and wind speed in the range of 15–20 m/s contribute largely to harvesting more energy.

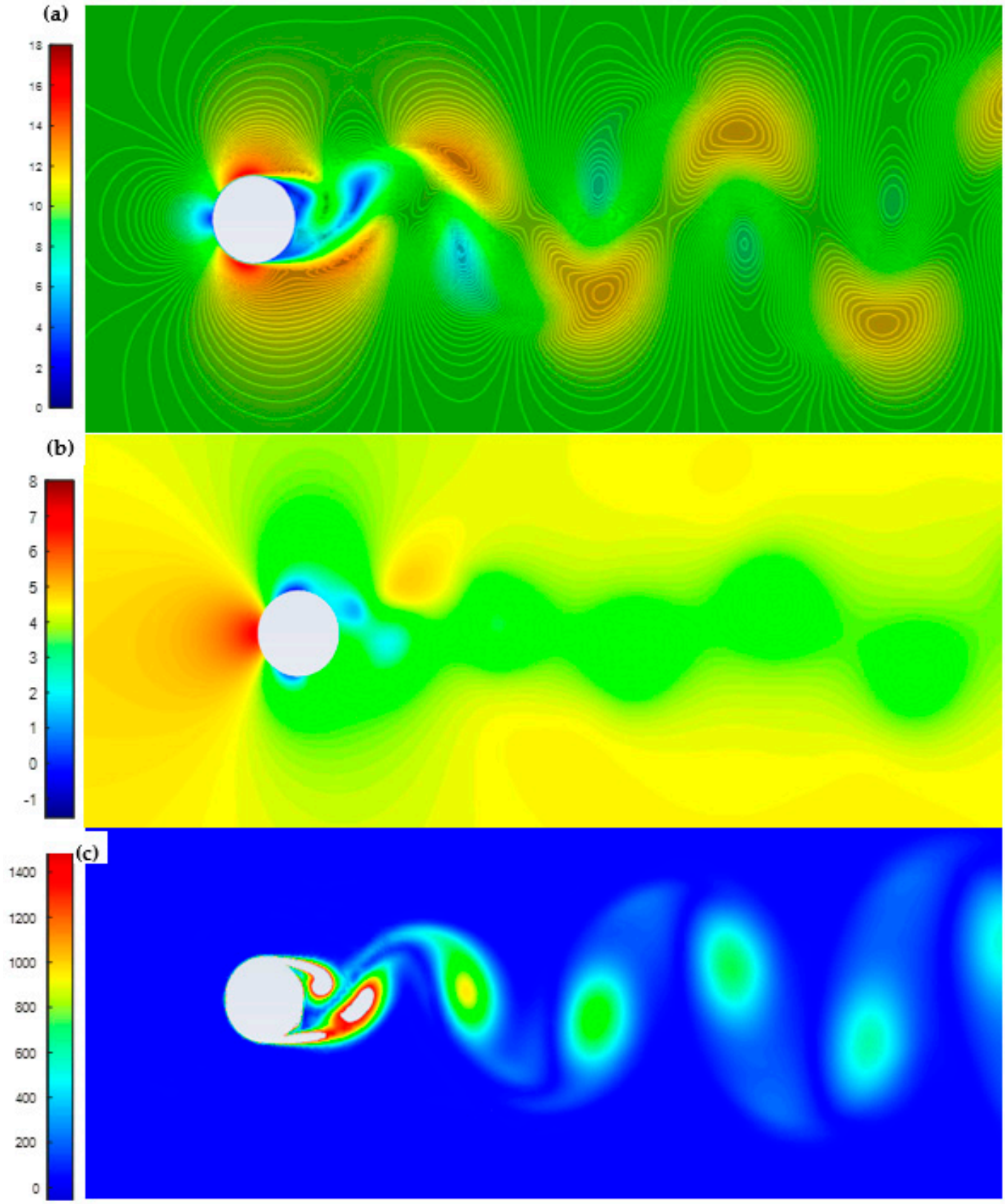


**Figure 3.** *Cont.*

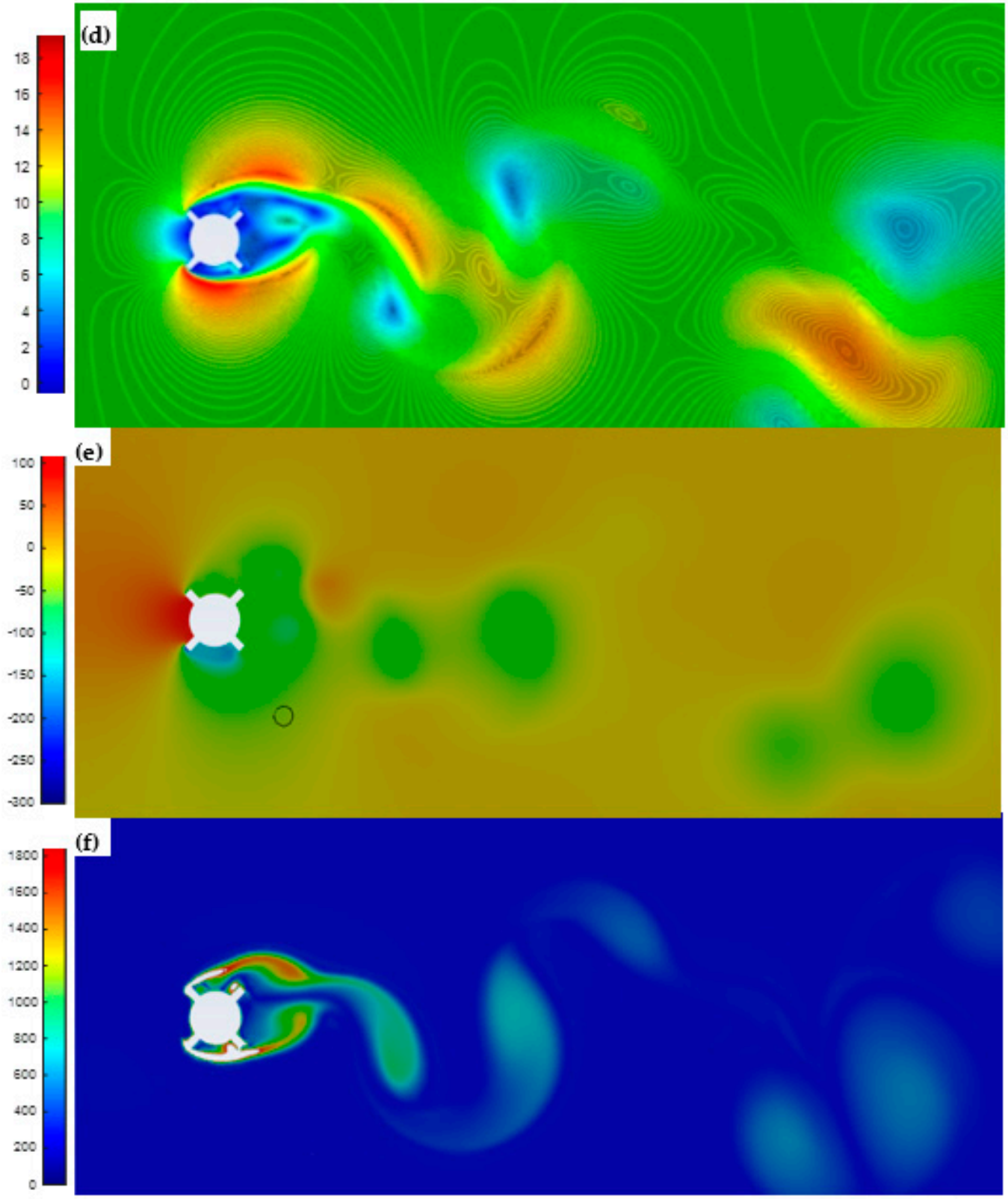


**Figure 3.** (**a**) Velocity contours for the simple cylinder at wind speed of 10 m/s, (**b**) pressure contours for simple cylinder at wind speed of 10 m/s, (**c**) vorticity contours for a simple cylinder at wind speed of 10 m/s, (**d**) velocity contours for the modified cylinder at wind speed of 10 m/s for simple cylinder, (**e**) pressure contours for the modified cylinder at wind speed of 10 m/s, and (**f**) vorticity contours for the modified cylinder at wind speed of 10 m/s.

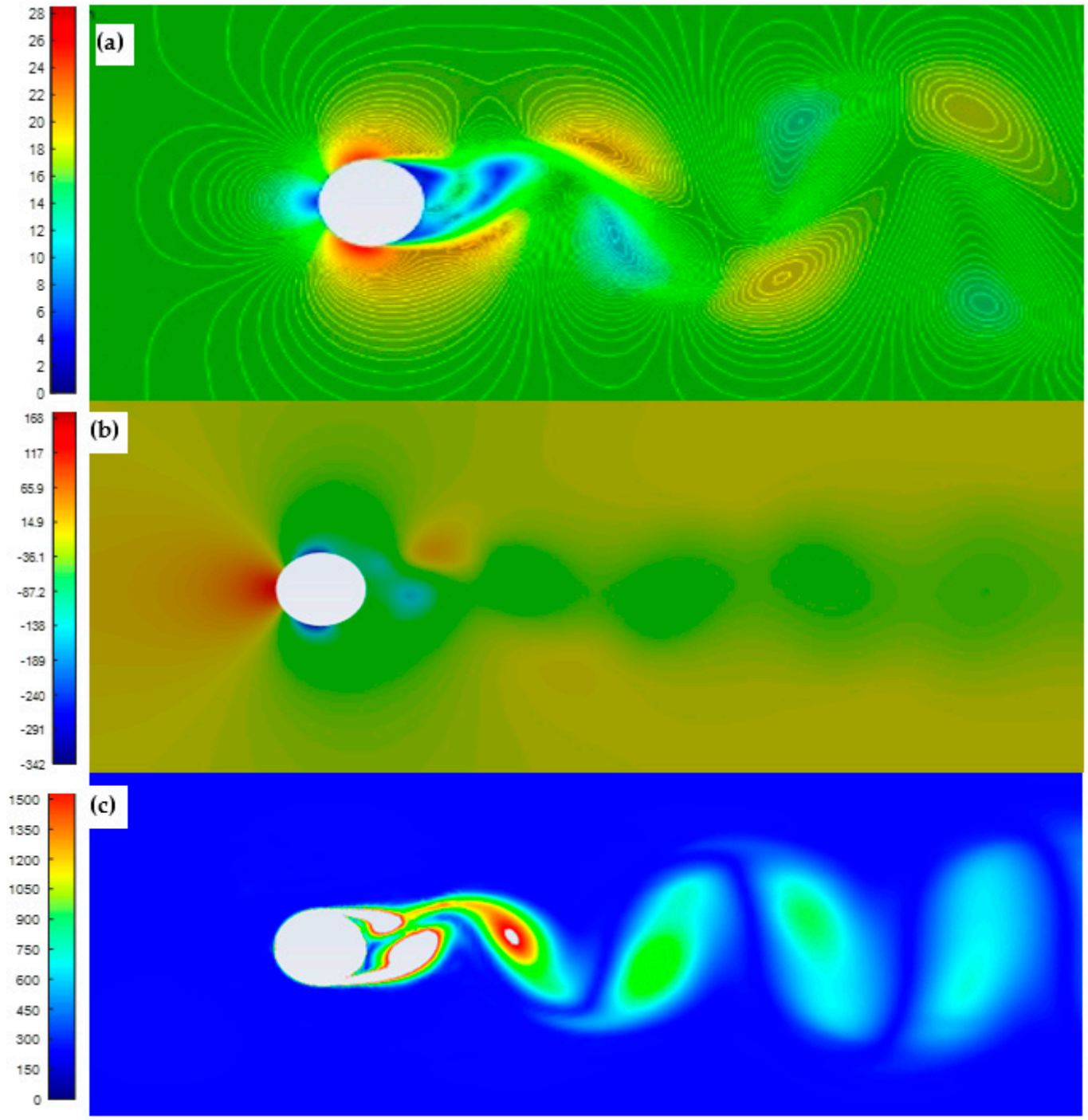


**Figure 4.** *Cont.*

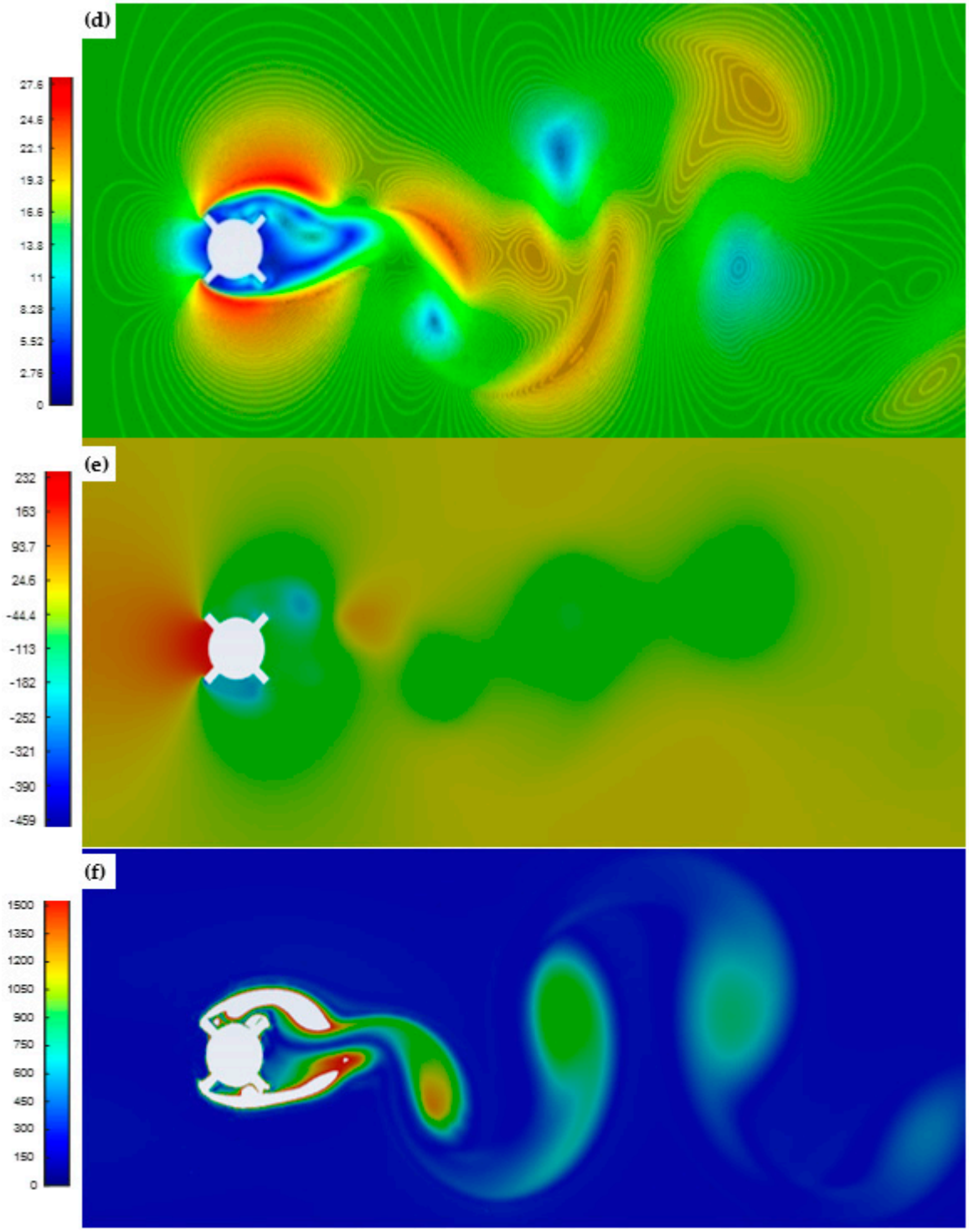


**Figure 4.** (**a**) Velocity contours for simple cylinder at wind speed of 15 m/s, (**b**) pressure contours for simple cylinder at wind speed of 15 m/s, (**c**) vorticity contours for simple cylinder at wind speed of 15 m/s, (**d**) velocity contours for modified cylinder at wind speed of 15 m/s for simple cylinder, (**e**) pressure contours for modified cylinder at wind speed of 20 m/s, and (**f**) vorticity contours for modified cylinder at wind speed of 15 m/s.

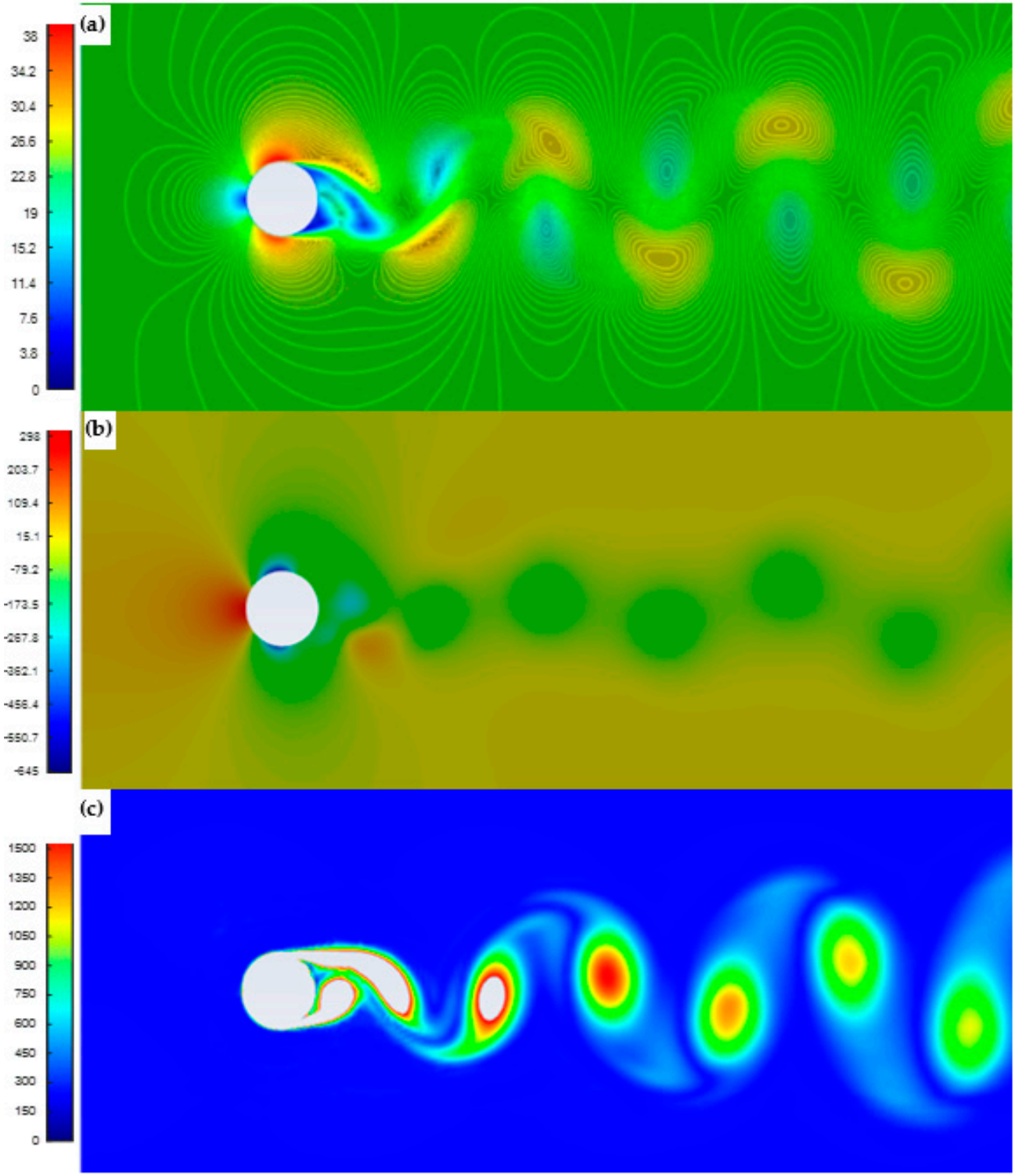


**Figure 5.** *Cont.*

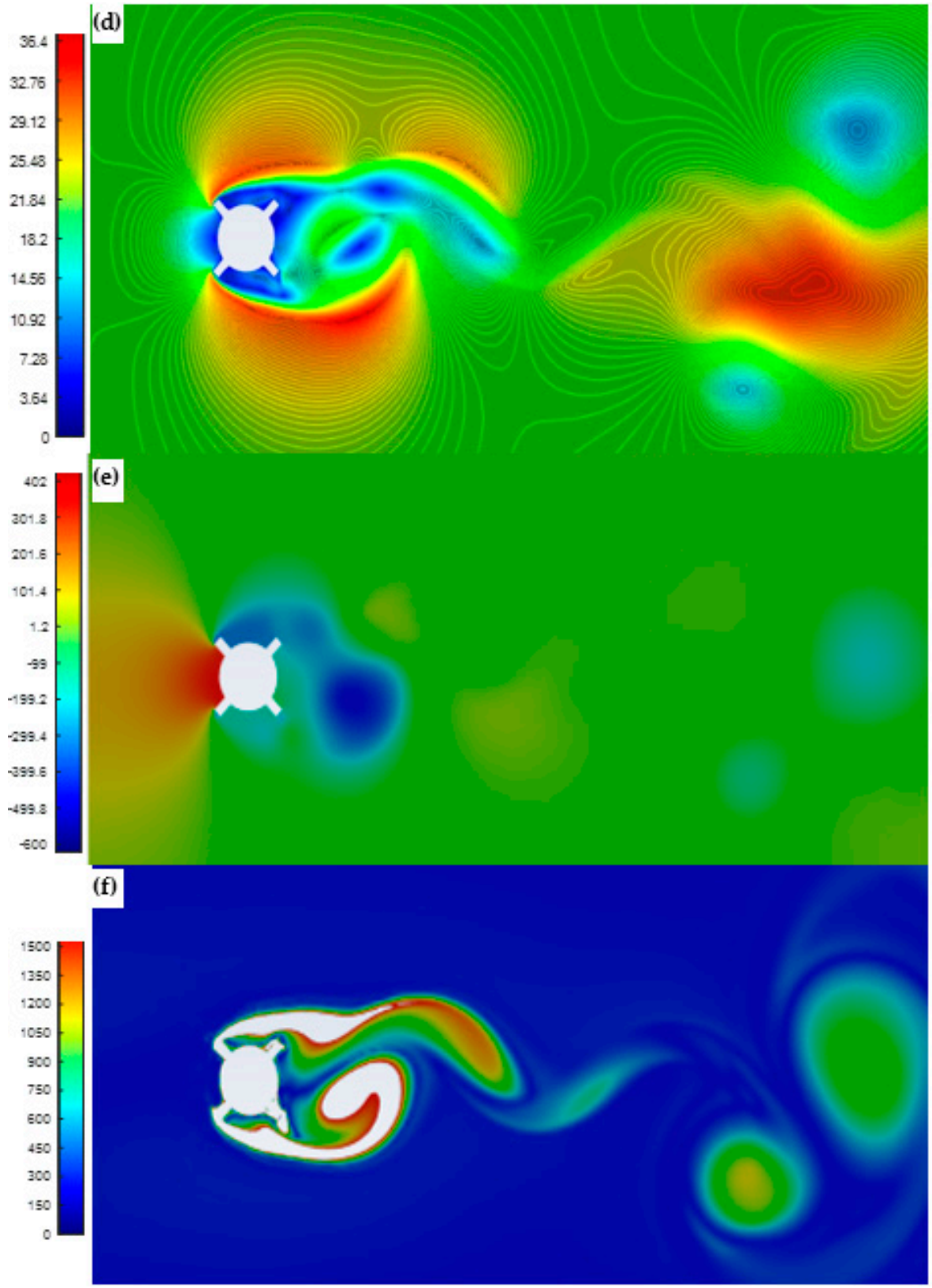


**Figure 5.** (**a**) Velocity contours for simple cylinder at wind speed of 20 m/s, (**b**) pressure contours for simple cylinder at wind speed of 20 m/s, (**c**) vorticity contours for simple cylinder at wind speed of 20 m/s, (**d**) velocity contours for modified cylinder at wind speed of 20 m/s for simple cylinder, (**e**) pressure contours for modified cylinder at wind speed of 20 m/s, and (**f**) vorticity contours for modified cylinder at wind speed of 20 m/s.

CFD simulations were carried out on the mast using its actual dimensions, including mast height, length, and diameter of the cylinder, and on the proposed design of both shapes of simple and complex cylinder geometries. The results showed that high pressure is created even at low wind speed, producing higher lift force and more vibrations. The intensity of vertices at low wind speed for complex shape design grows more extensive and even better at wind speeds equal to 15 and 20 m/s, as shown in Figure 6. A considerable amount of power can be harvested from the complex shape design at wind speeds as low as 5–20 m/s.

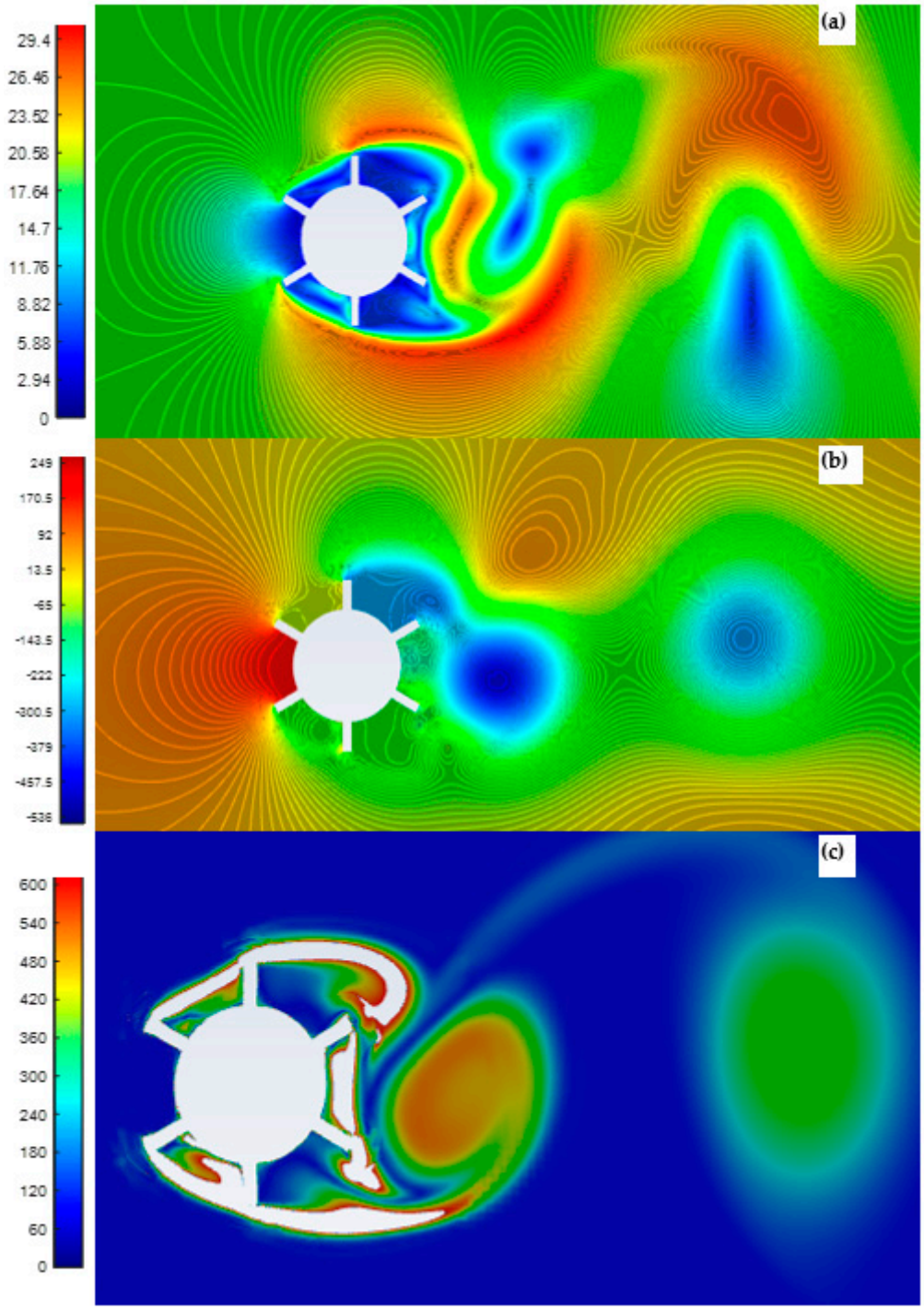


**Figure 6.** *Cont.*

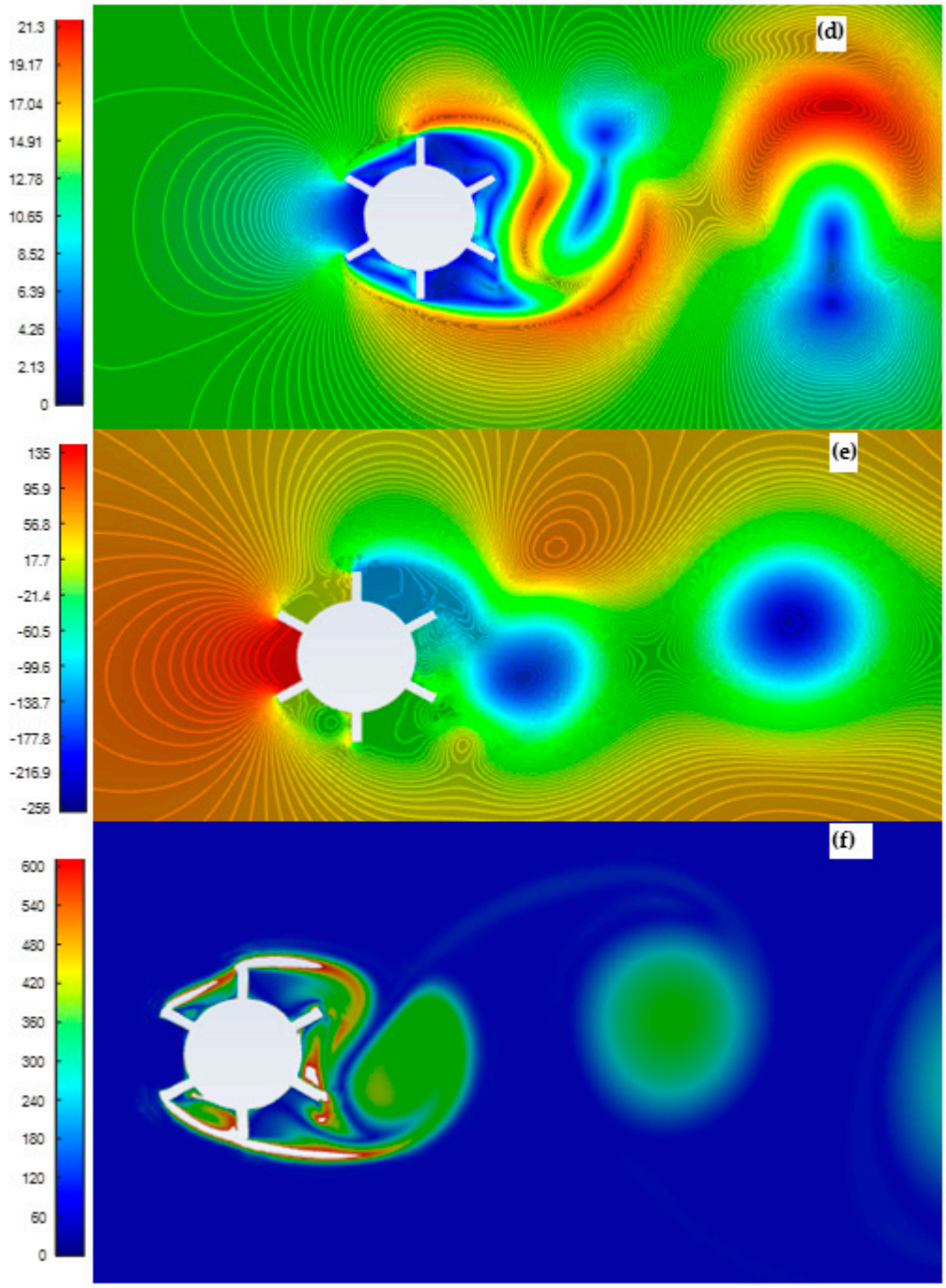


**Figure 6.** *Cont.*

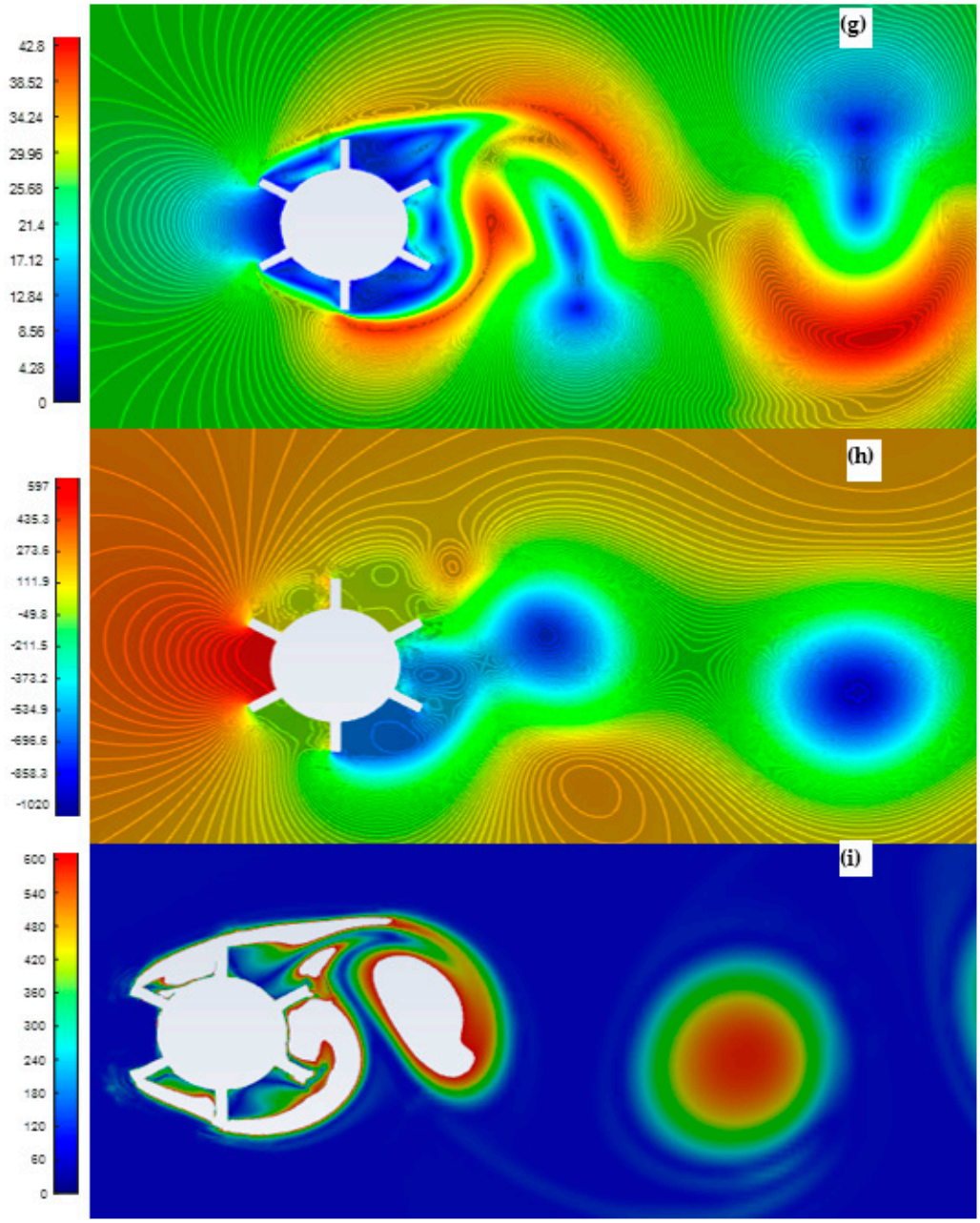


**Figure 6.** (**a**,**d**,**g**): velocity contours at wind speeds of 10, 15, and 20 m/s, respectively (range: [0, 20] m/s). (**b**,**e**,**h**): pressure contours at wind speeds of 10, 15, and 20 m/s, respectively. (**c**,**f**,**i**): vorticity contours at wind speeds of 10, 15, and 20 m/s, respectively.

## 4. Experimental Work Setup

The proposed designs were experimentally tested to determine how much energy can be harnessed from the proposed shape design at low wind speed. A piezoelectric sensor was attached to the proposed design's mast at three locations: top, middle, and bottom, as shown in Figure 2. The sensors were connected to voltammeters to read extracted voltage, which represents power. The mast angle is the angle of deviation of the mast from the airstream direction. Two angles were tested, at 0 and 5 degrees, to investigate the effect of the mast angle on the lift force and, hence, the harvested power. The prototypes of the suggested designs (simple cylinder and modified cylinder) were placed in an open-loop wind tunnel, as shown in Figures 7–9. The proposed prototypes were exposed to an airstream with different flow speeds, starting at 1 m/s up to 25 m/s. However, the focus in this study is the airstream speed in the range of 5 m/s to 20 m/s.

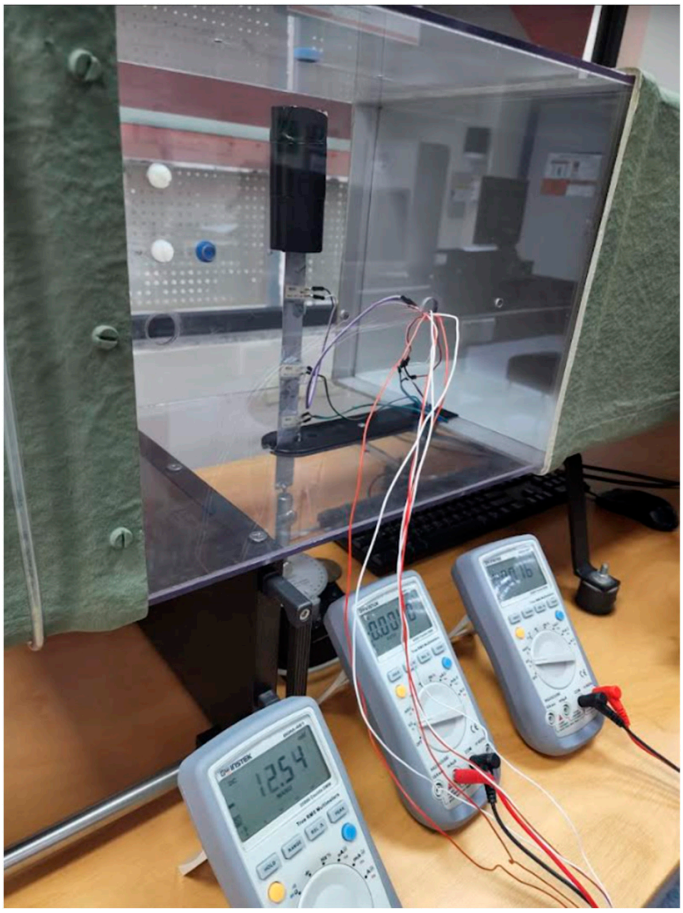

**Figure 7.** The experimental setup in a wind tunnel with piezoelectric sensors positioned at the tested locations.

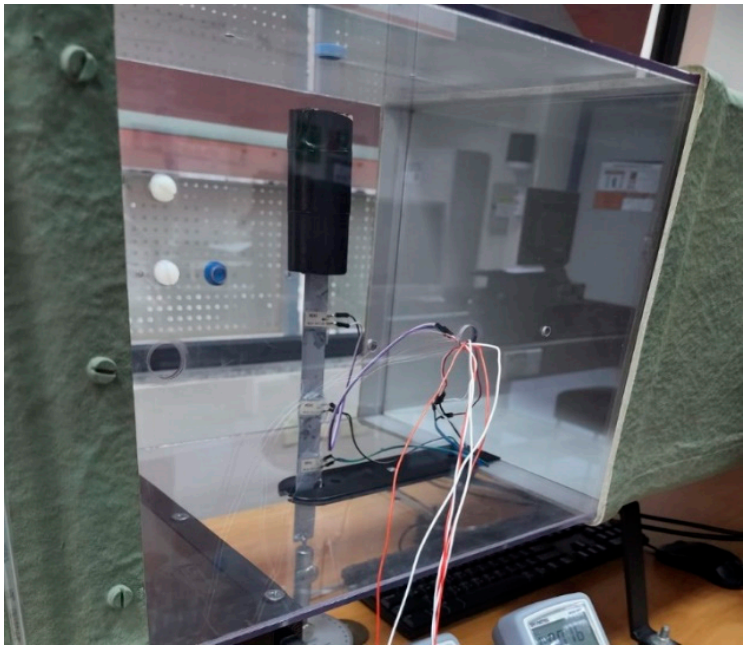

**Figure 8.** The proposed simple cylinder design experimental setup in wind tunnel with piezoelectric sensors positioned at the tested locations.

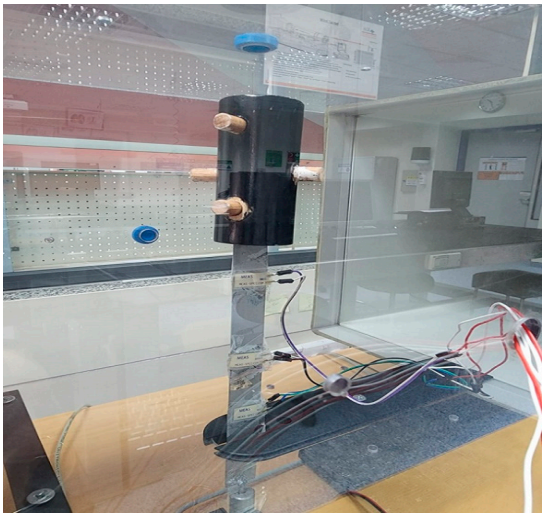

**Figure 9.** The proposed modified cylinder design experimental setup in a wind tunnel with piezoelectric sensors positioned at the tested locations.

## 5. Experimental Results

This section presents the results of the prepared experimental setup shown in Figure 8 for the simple cylinder and in Figure 9 for the modified cylinder. The data are related to the three locations of the piezoelectric component, i.e., top, middle, and bottom of that component, and for two different angles of attack, i.e., 0 and 5 degrees, and are presented in Tables A1–A4. As predicted by numerical results, increasing velocity increases the amount of applied force on the vortex generator. Furthermore, adding complexity increases the lift force slightly; however, this change was extensive in the numerical results, which could be related to the non-precise shape of the object added to the primary geometry and the accuracy of the measurement. Similarly, placing the piezoelectric component farther from the vortex generator object induces more electrical voltage in the piezoelectric element. Nevertheless, this phenomenon cannot be observed when the piezoelectric member is in the middle of the mast. The mast becomes an obstacle in the turbulent wind flow, which is neglected in the numerical simulation. This effect probably affects the wind flow around the mast and vortex generator object and enhances the vibrations of this part of the mast. Additionally, considering a constraint for the mast movement and fixing the mast to the ground changes the mast vibration pattern. Finally, it should be noted that the angle of attack almost does not impact the exerted lift force.

Maximum attainable power for each case when the piezoelectric sensor is located near the vortex generator utilizing Equation (5) is presented in Table 4. The amount of power obtained experimentally at different locations of the piezoelectric element is plotted in Figure 10.

**Table 4.** Calculated power attained for the piezoelectric component located at the top of the mast.

| Experimentally Tested Case | Maximum Attainable Power (nW) |
|---|---|
| Case 1: Simple cylinder at v = 10 m/s | 0.00011974 |
| Case 2: Simple cylinder at v= 15 m/s | 0.0010777 |
| Case 3: Simple cylinder at v= 20 m/s | 0.0043108 |
| Case 4: Modified cylinder at v= 10 m/s | 0.00026942 |
| Case 5: Modified cylinder at v= 15 m/s | 0.0024248 |
| Case 6: Modified cylinder at v= 20 m/s | 0.0187100 |
| Case 7: Modified cylinder: real-life dimensions at v = 10 m/s | 0.0681910 |
| Case 8: Modified cylinder: real-life dimensions at v = 15 m/s | 0.7946900 |
| Case 9: Modified cylinder: real-life dimensions at 20 = 10 m/s | 3.1247000 |

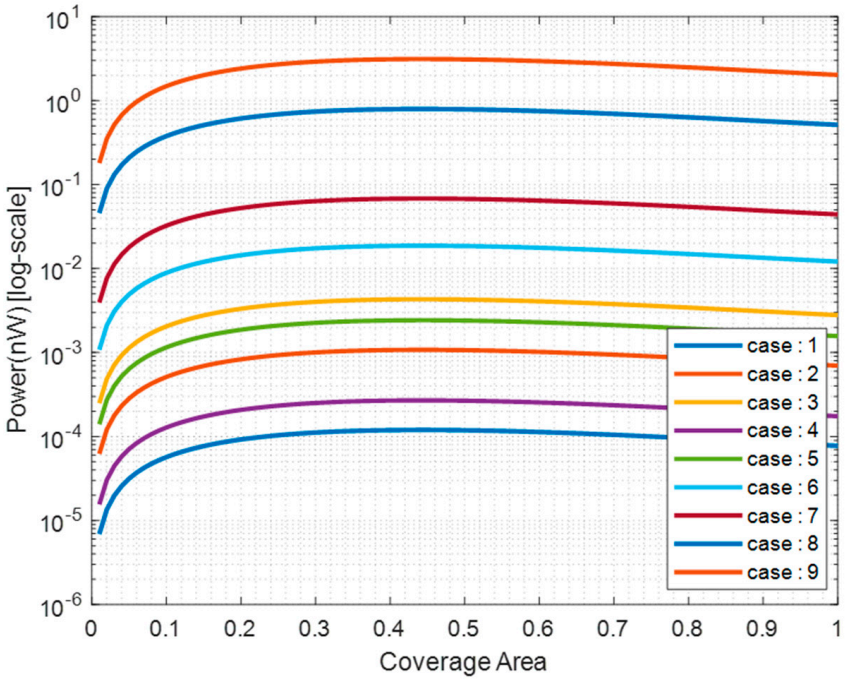


**Figure 10.** Output power attained for the piezoelectric component located at the top of the mast.

In addition, when the piezoelectric component is located at the bottom of the mast, more power can be harvested, as seen in Figure 11. The results are reported in Table 5 and plotted in Figure 11. The maximum harvested amount of energy is 212.473 nW at a wind speed of 20 m/s using a modified cylinder with real-life dimensions. This result is promising for small electronic devices and can later be improved to generate more power.

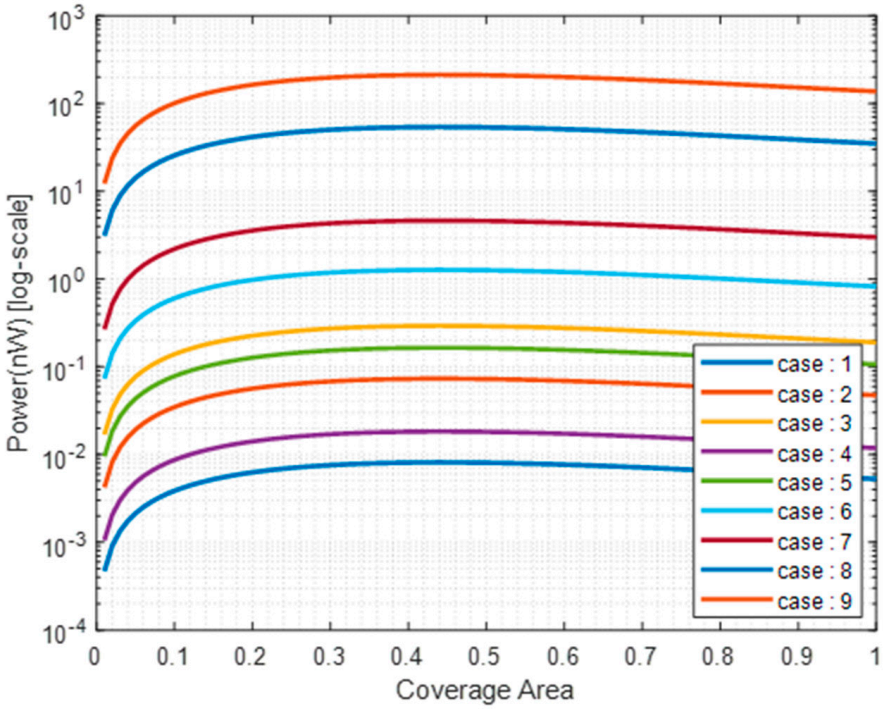


**Figure 11.** Output power for the piezoelectric component located at the bottom of the mast.

**Table 5.** Output power attained for the piezoelectric component located at the bottom of the mast.

| Experimentally Tested Case | Maximum Attainable Power (nW) |
|---|---|
| Case 1: Simple cylinder at v = 10 m/s | 0.0081424 |
| Case 2: Simple cylinder at v= 15 m/s | 0.073282 |
| Case 3: Simple cylinder at v= 20 m/s | 0.29313 |
| Case 4: Modified cylinder at v= 10 m/s | 0.01832 |
| Case 5: Modified cylinder at v= 15 m/s | 0.16488 |
| Case 6: Modified cylinder at v= 20 m/s | 1.2723 |
| Case 7: Modified cylinder: real-life dimensions at v = 10 m/s | 4.6369 |
| Case 8: Modified cylinder: real-life dimensions at v = 15 m/s | 54.038 |
| Case 9: Modified cylinder: real-life dimensions at 20 m/s | 212.473 |

It is evident from the above results that placing the piezoelectric component as far as possible from the vortex generator (bottom of the mast) provides more attainable power for the piezoelectric component.

As was expected, high wind velocity with the effect of adding complexity to the geometry, which are the contributing factors in the lift coefficient increase, positively affected the generated power by the piezoelectric component.

The experimental data obtained from the experimental work on the proposed designs are reported in Tables A1–A4. The experimental data represent the voltage readings at the piezoelectric locations on the mast and both the drag and lift forces that were experimentally monitored using a data acquisition system connected to the wind tunnel.

Figures 12–15 displays the amount of the harvested output voltage using the three sensors at angle of attack 0 and 5 degrees for both simple cylinder and complex cylinder. Figures 12–15 also displays the amount of lift and drag forces.

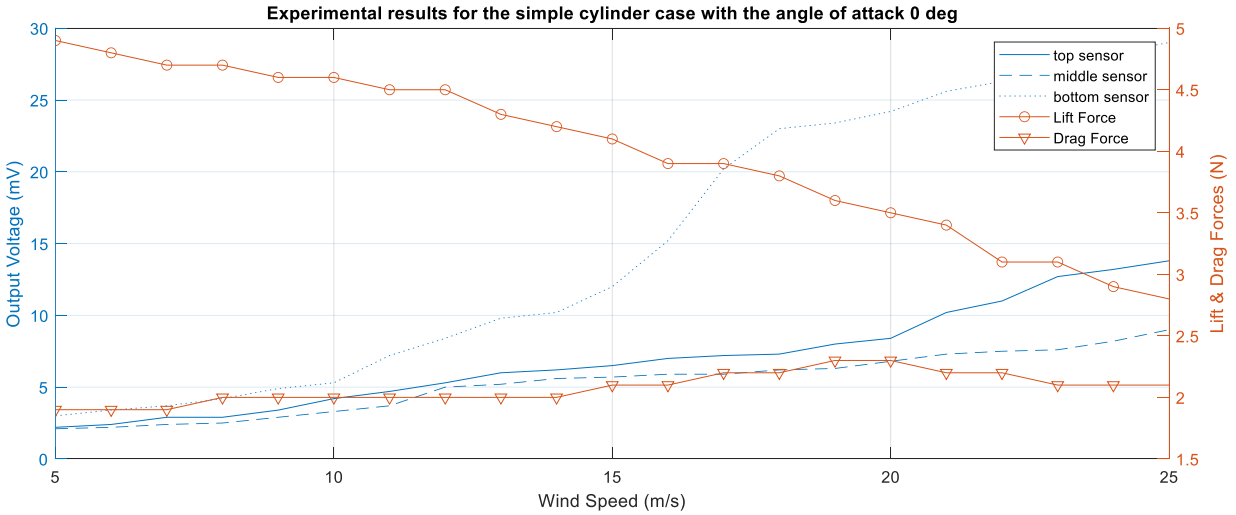


**Figure 12.** Experimental results for the simple cylinder case with the angle of attack at 0 deg.

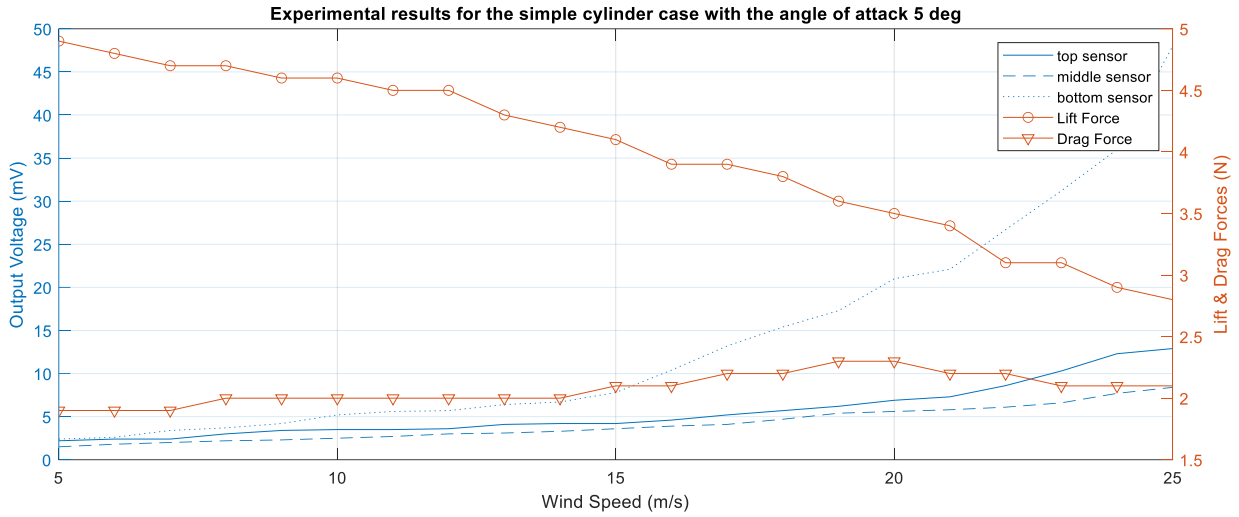


**Figure 13.** Experimental results for the simple cylinder case with the angle of attack at 5 deg.

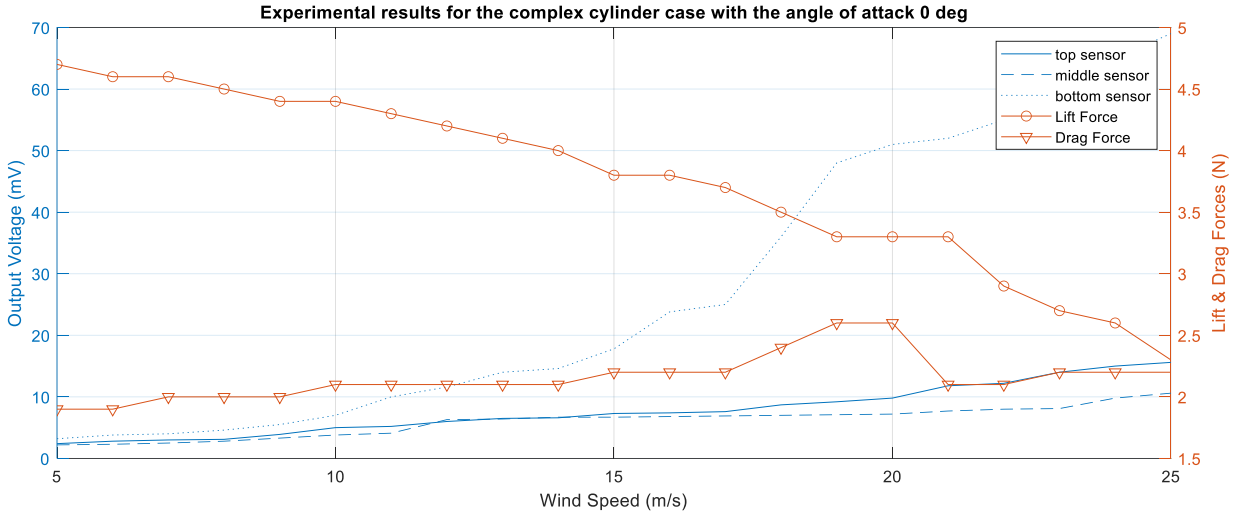


**Figure 14.** Experimental results for the complex cylinder case with the angle of attack at 0 deg.

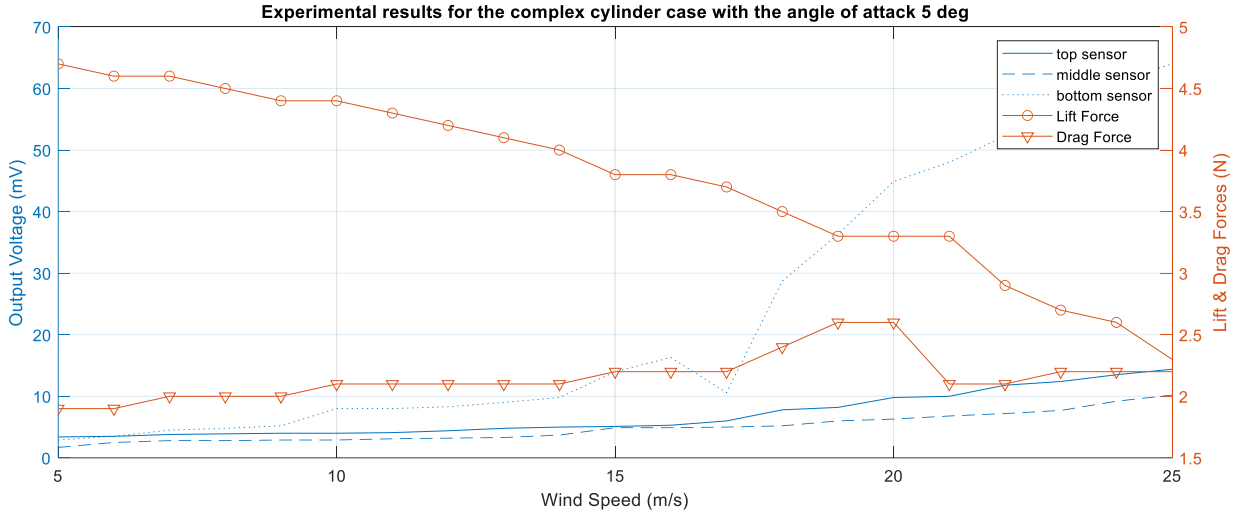


**Figure 15.** Experimental results for the complex cylinder case with mast angle of attack at 5 deg.

Figures A1–A3 present measured voltage from the piezoelectric sensors located at the top, middle, and bottom of the mast at different wind speeds with a mast angle of 0 degrees. The mast is now facing the flow stream with no deviation. Figure A4 displays the measured voltage of all simple cylinders using the sensors located at the top, middle, and bottom of the mast at an angle of 0 degrees.

The angle of the mast was adjusted to be 5 degrees, and experimental work was carried out to investigate the effect of the mast angle of attack on the attainable power. Figure A5 reports the experimentally harvested voltage and voltage readings using the piezoelectric sensor located at the top of the mast, at different wind speeds at a mast angle of 5 degrees, meaning the mast deviates by 5 degrees from the flow stream. Figure A6 reports the experimentally harvested voltage using the piezoelectric sensor located at the middle of the mast with a mast angle of 5 degrees. Figure A7 reports the experimentally harvested voltage using the piezoelectric sensor located at the bottom of the mast with a mast angle of 5 degrees. Figure A8 displays the harvested voltage of all simple cylinders using sensors located at the mast's top, middle, and bottom with a mast angle of 5 degrees.

Figure A8 clearly shows that a complex cylinder design with the piezoelectric sensor placed at the bottom of the mast produced the highest amount of energy. The measured voltages were 64 mV at a wind speed of 25 m/s and 44.9 mV at a wind speed of 20 m/s compared to the other designs at both angles and at all possible locations of the piezoelectric sensors. A simple cylinder design with the piezoelectric sensor placed at the bottom comes in second place, generating 49 mV at a wind speed of 25 m/s and 21 mV at a wind speed of 20 m/s. Therefore, based on the obtained results, it can be concluded that the complex cylinder vortex generator design is more feasible and efficient than the other tested designs. Moreover, the best option for the complex cylinder design configuration turned out to be at a 0-degree angle with the piezoelectric sensor placed at the bottom. There is a slight deviation in the results because the voltage reached 69 mV, while other trials reached maximum values of 64 mV at a 5-degree angle. The full-power harnesses achieved by complex cylinder design are 212 nW at a wind speed of 20 m/s.

## 6. Conclusions

This paper proposed a novel and new VIV design to harvest and convert mechanical energy to electric energy using a vortex-induced vibration technique. The proposed design is a bladeless elastic rod that vibrates when wind interacts with it. Out of the mechanical vibrations and rod oscillations, electric energy can be harvested through piezoelectric sensors attached to the mast at three locations. The design is environmentally friendly, with comparably good reliability. The effect of changing the vortex generator shape on the VIV phenomenon and VIV energy harvesting was investigated numerically and experimentally. Three different inlet wind velocities were investigated for three different vortex generator geometries: a simple cylinder, a modified cylinder, and a real-world-sized complex cylinder vortex generator. CFD simulations were performed to investigate the flow pattern and the generated vortices. Velocity, pressure, and vorticity contours were generated and analyzed. Piezoelectric sensors were utilized to measure generated power. Their optimal locations were also investigated. More importantly, the transient behavior of the lift coefficient over time is given for each case. The results of the numerical study demonstrate that increasing the inlet wind velocity increases the maximum magnitude of the lift coefficient, its frequency, and the time needed to reach the pseudo-steady situation in this problem, which has a transient nature. In addition, adding complexity to the cylinder geometry substantially enhances the maximum lift force applied to the vortex generators and can boost the efficiency of VIV energy harvesting. The trends of the numerical results are found to be in good agreement with those of the experimental tests. The experimental results show that the location of the piezoelectric sensor influences the amount of generated power. Increasing the distance from the vortex generator object does not directly increase the generated power, and this could be because the mast obstructed the wind flow around the vortex generator and the constraint for mast movement. If such designs are refined

and enhanced in terms of design geometry and the materials utilized in manufacturing the mast of the VIV design, a good quantity of power can be created. The developed and tested methods yielded good results.

**Author Contributions:** Conceptualization, Z.D. and A.Y.; Data curation, A.Y., H.S. and A.A. (Abdullah Alawadhi); Formal analysis, A.Y., A.A. (Abeer AlAnazi), H.S. and A.A. (Abdullah Alawadhi); Investigation, A.Y.; Methodology, A.Y.; Resources, Z.D., A.Y., M.E. and H.S.; Software, A.Y. and A.A. (Abeer AlAnazi); Supervision, A.Y.; Validation, A.A. (Abdullah Alawadhi); Visualization, A.Y., M.E.; Writing—original draft, A.Y.; Writing—review & editing, Z.D. and A.Y. All authors have read and agreed to the published version of the manuscript.

**Funding:** This research received no external funding.

**Institutional Review Board Statement:** Not applicable.

**Informed Consent Statement:** Not applicable.

**Data Availability Statement:** Not applicable.

**Conflicts of Interest:** The authors declare no conflict of interest.

## Appendix A. Experimental Results

**Table A1.** Experimental results for the simple cylinder case with the angle of attack at 0 deg.

| Velocity m/s | Top (mmV) | Middle (mmV) | Bottom (mmV) | Drag Force (N) | Lift Force (N) |
|---|---|---|---|---|---|
| 5 | 2.2 | 2.1 | 3 | 4.9 | 1.9 |
| 6 | 2.4 | 2.2 | 3.4 | 4.8 | 1.9 |
| 7 | 2.9 | 2.4 | 3.7 | 4.7 | 1.9 |
| 8 | 2.9 | 2.5 | 4.2 | 4.7 | 2 |
| 9 | 3.4 | 2.9 | 4.9 | 4.6 | 2 |
| 10 | 4.2 | 3.3 | 5.3 | 4.6 | 2 |
| 11 | 4.7 | 3.7 | 7.2 | 4.5 | 2 |
| 12 | 5.3 | 5 | 8.4 | 4.5 | 2 |
| 13 | 6 | 5.2 | 9.8 | 4.3 | 2 |
| 14 | 6.2 | 5.6 | 10.2 | 4.2 | 2 |
| 15 | 6.5 | 5.7 | 12 | 4.1 | 2.1 |
| 16 | 7 | 5.9 | 15.2 | 3.9 | 2.1 |
| 17 | 7.2 | 5.9 | 20.2 | 3.9 | 2.2 |
| 18 | 7.3 | 6.2 | 23 | 3.8 | 2.2 |
| 19 | 8 | 6.3 | 23.4 | 3.6 | 2.3 |
| 20 | 8.4 | 6.8 | 24.2 | 3.5 | 2.3 |
| 21 | 10.2 | 7.3 | 25.6 | 3.4 | 2.2 |
| 22 | 11 | 7.5 | 26.3 | 3.1 | 2.2 |
| 23 | 12.7 | 7.6 | 27.5 | 3.1 | 2.1 |
| 24 | 13.2 | 8.2 | 28.3 | 2.9 | 2.1 |
| 25 | 13.8 | 9 | 29 | 2.8 | 2.1 |

**Table A2.** Experimental results for the simple cylinder case with the angle of attack at 5 deg.

| Velocity (m/s) | Top (mmV) | Middle (mmV) | Bottom (mmV) | Drag Force (N) | Lift Force (N) |
|---|---|---|---|---|---|
| 5 | 2.2 | 1.5 | 2.4 | 4.9 | 1.9 |
| 6 | 2.4 | 1.8 | 2.6 | 4.8 | 1.9 |
| 7 | 2.4 | 2 | 3.4 | 4.7 | 1.9 |
| 8 | 3 | 2.2 | 3.7 | 4.7 | 2 |
| 9 | 3.4 | 2.3 | 4.2 | 4.6 | 2 |
| 10 | 3.5 | 2.5 | 5.2 | 4.6 | 2 |
| 11 | 3.5 | 2.7 | 5.6 | 4.5 | 2 |

**Table A2.** *Cont.*

| Velocity (m/s) | Top (mmV) | Middle (mmV) | Bottom (mmV) | Drag Force (N) | Lift Force (N) |
|---|---|---|---|---|---|
| 12 | 3.6 | 3 | 5.7 | 4.5 | 2 |
| 13 | 4.1 | 3.1 | 6.4 | 4.3 | 2 |
| 14 | 4.2 | 3.3 | 6.7 | 4.2 | 2 |
| 15 | 4.2 | 3.6 | 7.8 | 4.1 | 2.1 |
| 16 | 4.6 | 3.9 | 10.4 | 3.9 | 2.1 |
| 17 | 5.2 | 4.1 | 13.2 | 3.9 | 2.2 |
| 18 | 5.7 | 4.7 | 15.4 | 3.8 | 2.2 |
| 19 | 6.2 | 5.4 | 17.3 | 3.6 | 2.3 |
| 20 | 6.9 | 5.6 | 21 | 3.5 | 2.3 |
| 21 | 7.3 | 5.8 | 22.1 | 3.4 | 2.2 |
| 22 | 8.6 | 6.1 | 26.7 | 3.1 | 2.2 |
| 23 | 10.3 | 6.6 | 31.2 | 3.1 | 2.1 |
| 24 | 12.3 | 7.7 | 36 | 2.9 | 2.1 |
| 25 | 12.9 | 8.4 | 48 | 2.8 | 2.1 |

**Table A3.** Experimental results for the complex cylinder case with the angle of attack at 0 deg.

| Velocity (m/s) | Top (mmV) | Middle (mmV) | Bottom (mmV) | Drag Force (N) | Lift Force (N) |
|---|---|---|---|---|---|
| 5 | 2.4 | 2.2 | 3.2 | 4.7 | 1.9 |
| 6 | 2.8 | 2.3 | 3.8 | 4.6 | 1.9 |
| 7 | 3 | 2.5 | 4 | 4.6 | 2 |
| 8 | 3.1 | 2.8 | 4.6 | 4.5 | 2 |
| 9 | 3.9 | 3.3 | 5.5 | 4.4 | 2 |
| 10 | 5 | 3.8 | 7 | 4.4 | 2.1 |
| 11 | 5.2 | 4.1 | 10 | 4.3 | 2.1 |
| 12 | 6 | 6.3 | 11.6 | 4.2 | 2.1 |
| 13 | 6.5 | 6.4 | 14 | 4.1 | 2.1 |
| 14 | 6.6 | 6.7 | 14.6 | 4 | 2.1 |
| 15 | 7.3 | 6.7 | 17.8 | 3.8 | 2.2 |
| 16 | 7.4 | 6.8 | 23.8 | 3.8 | 2.2 |
| 17 | 7.6 | 6.9 | 25 | 3.7 | 2.2 |
| 18 | 8.7 | 7 | 36 | 3.5 | 2.4 |
| 19 | 9.2 | 7.1 | 48 | 3.3 | 2.6 |
| 20 | 9.8 | 7.2 | 51 | 3.3 | 2.6 |
| 21 | 11.8 | 7.7 | 52 | 3.3 | 2.1 |
| 22 | 12.2 | 8 | 55 | 2.9 | 2.1 |
| 23 | 14 | 8.1 | 59 | 2.7 | 2.2 |
| 24 | 15 | 9.8 | 65 | 2.6 | 2.2 |
| 25 | 15.6 | 10.6 | 69 | 2.3 | 2.2 |

**Table A4.** Experimental results for the complex cylinder case with mast angle of attack at 5 deg.

| Velocity (m/s) | Top (mmV) | Middle (mmV) | Bottom (mmV) | Drag Force (N) | Lift Force (N) |
|---|---|---|---|---|---|
| 5 | 3.4 | 1.7 | 2.9 | 4.7 | 1.9 |
| 6 | 3.5 | 2.5 | 3.5 | 4.6 | 1.9 |
| 7 | 3.8 | 2.8 | 4.5 | 4.6 | 2 |
| 8 | 3.9 | 2.8 | 4.8 | 4.5 | 2 |
| 9 | 4 | 2.9 | 5.2 | 4.4 | 2 |
| 10 | 4 | 2.9 | 8 | 4.4 | 2.1 |
| 11 | 4.1 | 3.1 | 8 | 4.3 | 2.1 |
| 12 | 4.4 | 3.2 | 8.3 | 4.2 | 2.1 |
| 13 | 4.8 | 3.3 | 9 | 4.1 | 2.1 |

**Table A4.** *Cont.*

| Velocity (m/s) | Top (mmV) | Middle (mmV) | Bottom (mmV) | Drag Force (N) | Lift Force (N) |
|---|---|---|---|---|---|
| 14 | 5 | 3.7 | 9.8 | 4 | 2.1 |
| 15 | 5.1 | 4.9 | 14 | 3.8 | 2.2 |
| 16 | 5.3 | 4.9 | 16.3 | 3.8 | 2.2 |
| 17 | 6 | 5 | 10.6 | 3.7 | 2.2 |
| 18 | 7.8 | 5.2 | 28.7 | 3.5 | 2.4 |
| 19 | 8.2 | 6 | 36.3 | 3.3 | 2.6 |
| 20 | 9.8 | 6.3 | 44.9 | 3.3 | 2.6 |
| 21 | 10 | 6.8 | 48 | 3.3 | 2.1 |
| 22 | 11.8 | 7.2 | 52.3 | 2.9 | 2.1 |
| 23 | 12.4 | 7.7 | 59.7 | 2.7 | 2.2 |
| 24 | 13.5 | 9.2 | 61 | 2.6 | 2.2 |
| 25 | 14.4 | 10.2 | 64 | 2.3 | 2.2 |

## Appendix B

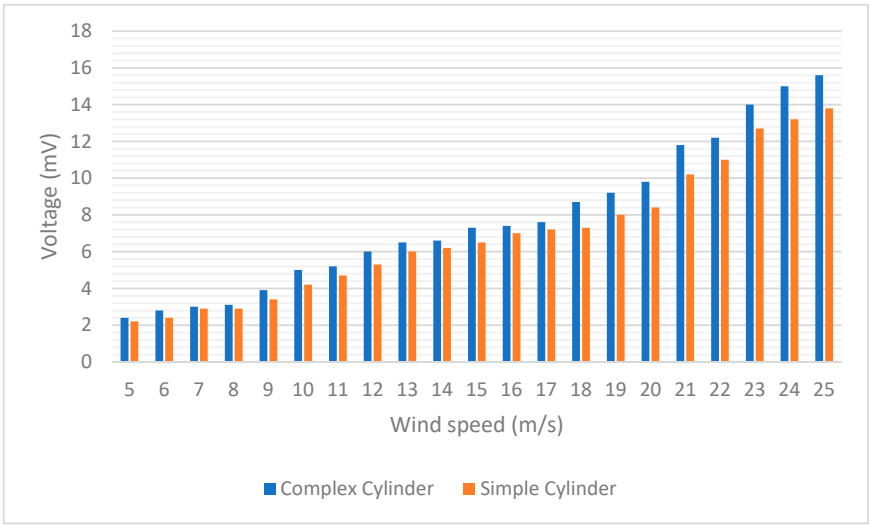


**Figure A1.** Voltage vs. wind speed (piezoelectric sensor is located at the top of the mast with mast angle at 0 degrees).

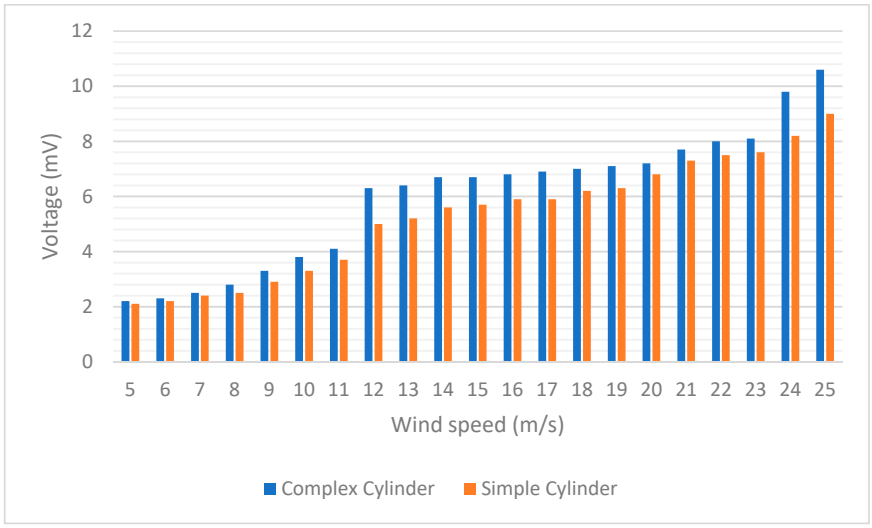


**Figure A2.** Voltage vs. wind speed (piezoelectric sensor is located at the middle of the mast with mast angle at 0 degrees).

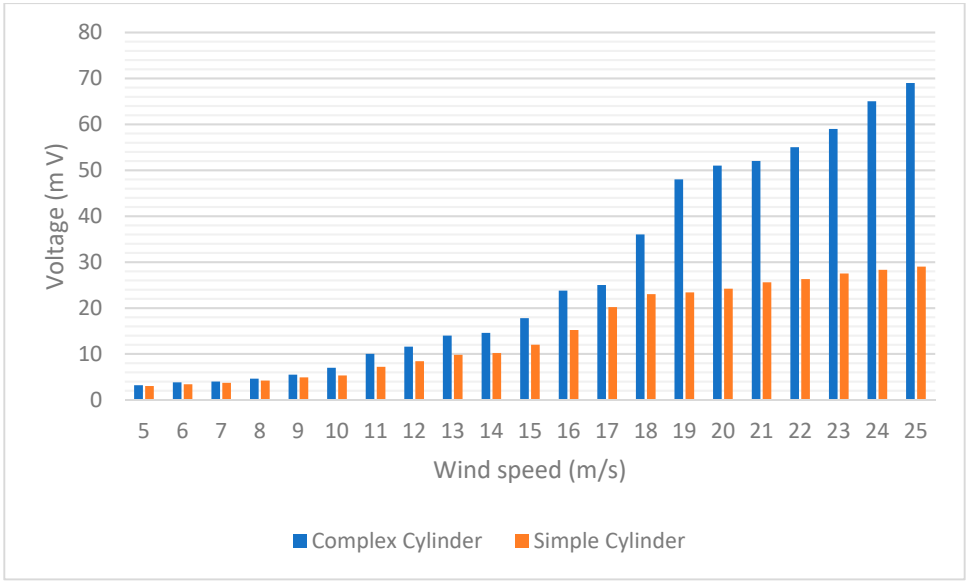


**Figure A3.** Voltage vs. wind speed (piezoelectric sensor is located at the bottom of the mast with mast angle at 0 degrees).

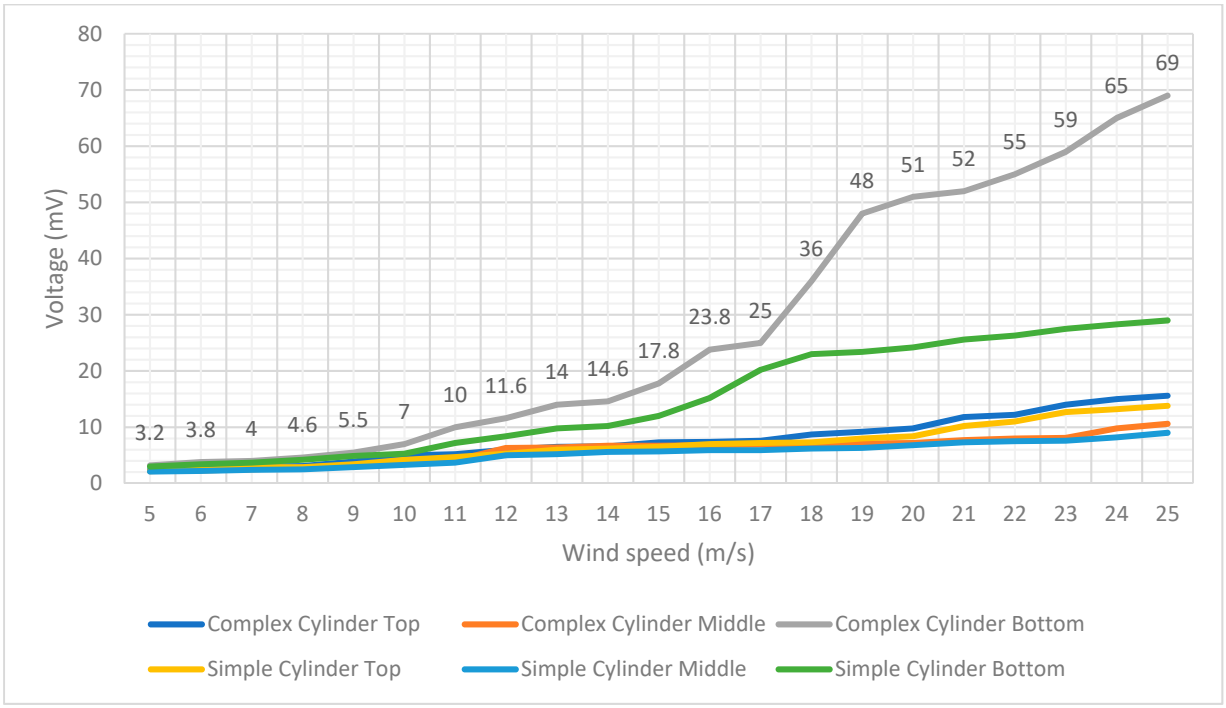


**Figure A4.** Combined results for case 1 (mast angle at 0 degrees).

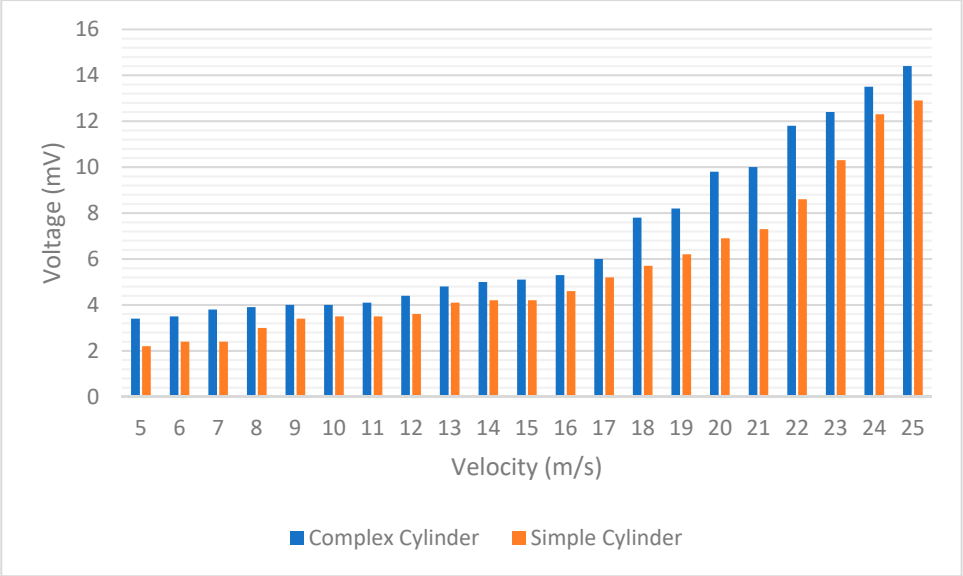


**Figure A5.** Voltage vs. velocity (piezoelectric sensor is located at the top of the mast with mast angle at 5 degrees).

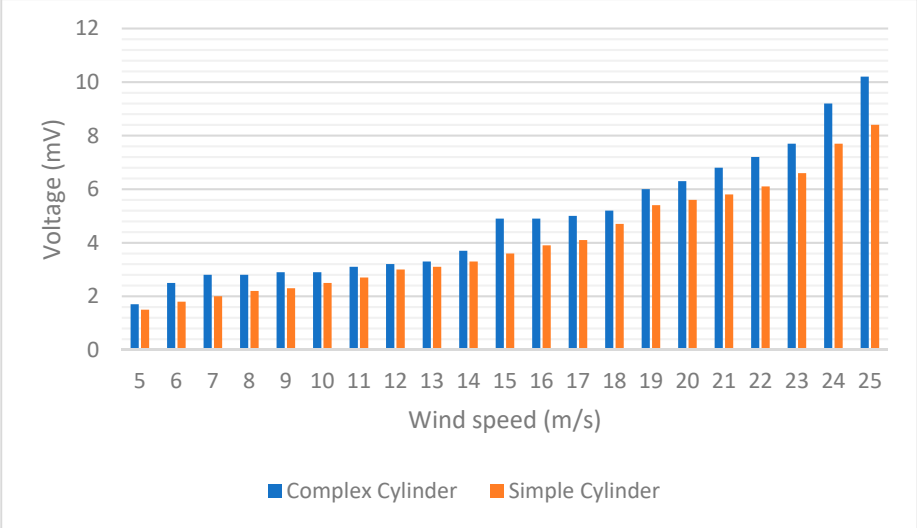


**Figure A6.** Voltage vs. velocity (piezoelectric sensor is located at the middle of the mast with mast angle at 5 degrees).

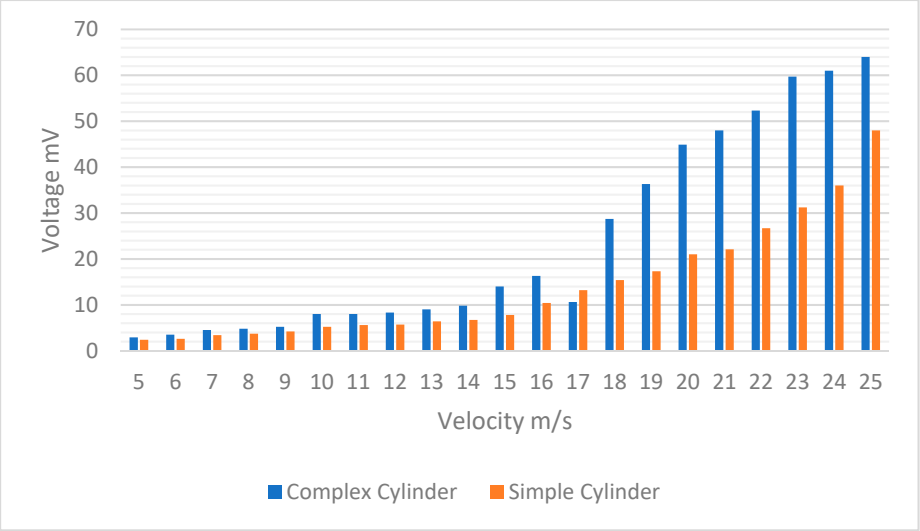


**Figure A7.** Voltage vs. velocity (piezoelectric sensor is located at the bottom of the mast with mast angle at 5 degrees).

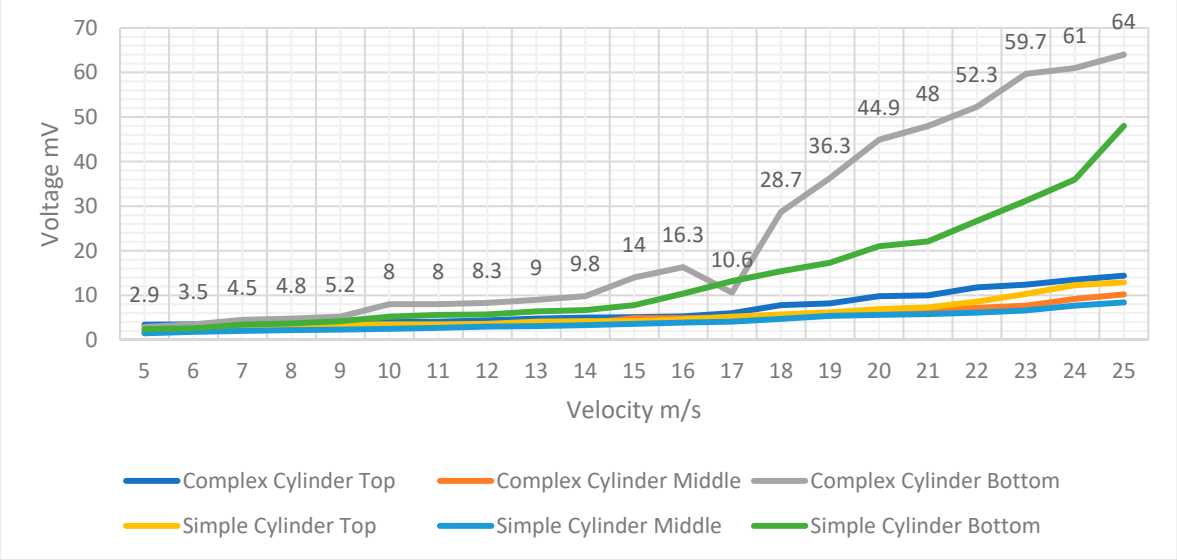


**Figure A8.** Combined results for case 2 (mast angle at 5 degrees).

## References

1. Sarpkaya, T. A critical review of the intrinsic nature of vortex-induced vibrations. *J. Fluids Struct.* **2004**, *19*, 389–447. [CrossRef]
2. Abdelkefi, A. Aeroelastic energy harvesting: A review. *Int. J. Eng. Sci.* **2016**, *100*, 112–135. [CrossRef]
3. Barrero-Gil, A.; Alonso, G.; Sanz-Andres, A. Energy harvesting from transverse galloping. *J. Sound Vib.* **2010**, *329*, 2873–2883. [CrossRef]
4. Lee, Y.J.; Qi, Y.; Zhou, G.; Lua, K.B. Vortex-induced vibration wind energy harvesting by piezoelectric MEMS device in formation. *Sci. Rep.* **2019**, *9*, 20404–20411. [CrossRef] [PubMed]
5. Abdelkefi, A.; Hajj, M.R.; Nayfeh, A.H. Piezoelectric energy harvesting from transverse galloping of bluff bodies. *Smart Mater. Struct.* **2013**, *22*, 015014. [CrossRef]
6. Li, X.; Bi, C.; Li, Z.; Liu, B.; Wang, T.; Zhang, S. A Piezoelectric and Electromagnetic Hybrid Galloping Energy Harvester with the Magnet Embedded in the Bluff Body. *Micromachines* **2021**, *12*, 626. [CrossRef] [PubMed]
7. Akaydın, H.D.; Elvin, N.; Andreopoulos, Y. Wake of a cylinder: A paradigm for energy harvesting. *Exp. Fluids* **2010**, *49*, 291–304. [CrossRef]
8. Mehmood, A.; Abdelkefi, A.; Akhtar, I.; Nayfeh, A.; Nuhait, A.; Hajj, M. Linear and nonlinear active feedback controls for vortex-induced vibrations of circular cylinders. *J. Vib. Control* **2012**, *20*, 1137–1147. [CrossRef]
9. Akaydin, H.D.; Elvin, N.; Andreopoulos, Y. The performance of a self-excited fluidic energy harvester. *Smart Mater. Struct.* **2012**, *21*, 025007. [CrossRef]

10. Dai, H.L.; Abdelkefi, A.; Yang, Y.; Wang, L. Orientation of bluff body for designing efficient energy harvesters from vortex-induced vibrations. *Appl. Phys. Lett.* **2016**, *108*, 053902. [CrossRef]
11. Masana, R.; Daqaq, M.F. Relative performance of a vibratory energy harvester in mono- and bi-stable potentials. *J. Sound Vib.* **2011**, *330*, 6036–6052. [CrossRef]
12. Naseer, R.; Dai, H.; Abdelkefi, A.; Wang, L. Comparative Study of Piezoelectric Vortex-Induced Vibration-Based Energy Harvesters with Multi-Stability Characteristics. *Energies* **2020**, *13*, 71. [CrossRef]
13. Su, W.-J.; Wang, Z.-S. Development of a Non-Linear Bi-Directional Vortex-Induced Piezoelectric Energy Harvester with Magnetic Interaction. *Sensors* **2021**, *21*, 2299. [CrossRef]
14. Dai, H.L.; Abdelkefi, A.; Javed, U.; Wang, L. Modeling and performance of electromagnetic energy harvesting from galloping oscillations. *Smart Mater. Struct.* **2015**, *24*, 5012. [CrossRef]
15. De Marqui, C., Jr.; Erturk, A. Electroaeroelastic analysis of airfoil-based wind energy harvesting using piezoelectric transduction and electromagnetic induction. *J. Intell. Mater. Syst. Struct.* **2012**, *24*, 846–854. [CrossRef]
16. Minazara, E.; France, S.U.D.C.-P.; Vasic, D.; Costa, F. Piezoelectric generator harvesting bike vibrations energy to supply portable devices. *Renew. Energy Power Qual. J.* **2008**, *1*, 508–513. [CrossRef]
17. Jayarathne, W.M.; Nimansala, W.A.T.; Adikary, S.U. Development of a Vibration Energy Harvesting Device Using Piezoelectric Sensors. In Proceedings of the Moratuwa Engineering Research Conference (MERCon), Moratuwa, SiriLanka, 30 May–1 June 2018; pp. 197–202.
18. Ishihara, T.; Li, T. Numerical study on suppression of vortex-induced vibration of circular cylinder by helical wires. *J. Wind Eng. Ind. Aerodyn.* **2020**, *197*, 104081. [CrossRef]
19. Li, T.; Ishihara, T. Numerical study on wake galloping of tandem circular cylinders considering the effects of mass and spacing ratios. *J. Wind Eng. Ind. Aerodyn.* **2021**, *210*, 104536. [CrossRef]